4.2 Heterogeneous Catalysis on a Monocrystalline Surface

4.2.1 The Data Sets Examined

The data sets[13] that were examined are the output of computer simulations of the dynamics for the one-dimensional case using the equations 2.31,2.32 and 2.33. Periodic boundary conditions were used in all simulations. The initial condition is a cosine wave in the spatial coordinate. This makes sure that simulations using identical parameter sets always lead to the same stationary dynamics. The simulation used a discretization with 1000 spatial points. The dimensionless variable corresponding to the covering with carbon monoxide was recorded at 100 locations and after every 160th timestep. The global data was recorded after every 16th timestep. The sample intervals are denoted with Δ_x and Δ_t in what follows.

The parameters used correspond to a experimental setup with a partial pressure in the inlet for oxygen $p_{O_2} = 1.17 \cdot 10^{-4}\, Torr$ and for carbon monoxide $p_{CO} = 4 \cdot 10^{-5}\, Torr$, a temperature $T = 545\, K$, a gas flow $J_{io} = 360\, l/s$ and a reactor volume $V = 55\, l$. For the volume of the monolayer V_{ML} see table 4.3

The data sets used include the transient phase.

abbreviation	V_{ML} [l]	type of dynamics
A	0.650	periodic
B	0.640	torus
C	0.620	temporal chaos
D	0.615	weak turbulence

Table 4.3: **The data sets examined.**

[13]All data samples for this system are courtesy of Dipl. Phys. Martin Falcke.

4.2.2 Analysis of the Global Data

Figures 4.24...4.27 show plots of the global data sets A...D including the transient phase.

The transient in A is an exponentially decaying amplitude modulation which seems to disappear only at the very end of plot in figure 4.24.

For B the transient cannot be recognized in the temporal profile (figure 4.25), but the maximum map of the whole data set[14] (figure 4.41, top) shows that the (toroidal) transient does only disappear at the end of the data set. The maximum map of the last 5000 samples (figure 4.41, bottom) could belong to a folded limit cycle with eleven loops. But also a toroidal dynamics with an irrational frequency ratio close to eleven can, due to the finite time of observation, produces this kind of maximum map. The data set B will be considered as toroidal dynamics in what follows. From the temporal profile alone one might have guessed a much shorter time of transient behavior than what the maximum map indicates.

The transient of C can be observed up to about sample number 10000 in the temporal plot. The maximum map (figure 4.42, top) does not help to find the transient time here because one does not know the pattern for the stationary case. The maximum map of the last 5000 samples indicates that the stationary case is chaotic but close to a limit cycle of period ratio eleven. For the further analysis the last 17000 of the total 31500 samples were considered as 'transient free'. As will be shown later the amount of transient remaining in this data set and even its form can be deduced from the empirical orthogonal functions (and their mode amplitudes) of the spatio-temporal data.

The global data for D (temporal plot in figure 4.27) does not allow to tell wether one observes stationary behavior at all. Indeed at the times of about $t = 6000$ and $t = 9500$ the stripe pattern in the global data changes. There seems to be a stationary pattern for times greater than $t = 9500$, in a computer simulation for times up to $t = 95000$ no more changes in the pattern could be observed. Here it seems to be impossible to draw any statement about the transient neither directly from the global data nor from the maximum map.

The histogram in figure 4.28 which belongs to data set A is typical for a periodic oscillation[15]. The modulated oscillation of data set B leads to the histogram shown in figure 4.29. For the chaotic global data sets C and D the distribution is more broadened (histograms in figures 4.30 and 4.31). A strictly periodic signal with greater modulation than B would lead to similar histograms.

Figures 4.32...4.35 show plots of the Fourier transforms of the global data sets. In all cases Welch windowing (cf. chapter 3.21) was used to avoid clip effects. The power spectrum of data set A shows purely periodic behavior with harmonics. The spectrum of B is typical for a torus with the ratio of the two dominant frequencies very close[16] to

[14] Data set B consists of 31500 samples. Note that the sampling rate in time for the global data is ten times higher than for the spatio-temporal data.

[15] For a harmonic oscillation the histogram should look like a plot of the function $1/\sqrt{1-x^2}$.

[16] If the ratio were exactly equal to an integer the dynamics had to be considered as a limit cycle.

1:11. For finite observation times a limit cycle and a torus with a frequency ratio very close to that of the limit cycle cannot be distinguished.

The spectrum for data set C looks similar to that of data set B but there are regions with a continuous power spectral density[17]. These do, together with the fact that the data comes from a purely deterministic system, indicate chaos.

There are numerous sidebands in the power spectrum of data set C, which may be generated in two different ways: by an amplitude modulation with a non-sinusidal function[18] or by a frequency modulation. Here the sidebands are mainly due to amplitude modulation ($m_a = 20\%$), the frequency modulation is approximately ten times weaker. The signal is not symmetric with respect to zero so the relations 3.62 and 3.61 lead do different results for the contours of the local minima and maxima. Using the maxima one finds for the amplitude modulation $m_a = 40\%$ and for the frequency modulation $m_f = 3.3\%$. The same calculations executed for the sequence of local minima lead to $m_a = 20\%$ and $m_f = 1.8\%$. For the amplitude modulation one has to take the ratio of the smallest and the biggest amplitude in the temporal profile which leads to $m_a = 20\%$. Strictly spoken nothing can be said about the frequency modulation, not even that it takes a value between those given above. It is possible to construct 'pathological' modulated signals that give arbitrary triples of values for the frequency modulation depending whether one uses maxima, minima or zero crossings for its determination[19].

The spectrum of D is the most irregular among these data sets, but its structure is still similar to the other spectra. The ratio of the two main frequencies is approximately 1:9. Again the continuous regions in the power spectral density indicate chaos.

Predictions with autoregressive models were used to characterise the amount of linear correlation in the data. As the data sets are very periodic in all cases the amplitude contours were used for the predictions. In the amplitude contour the main periodicity of a time series is removed and it is easier to fit linear models to that data because its autocorrelation function usually falls more rapidly.

Figures 4.38 show realizations of autoregressive models of the orders 5,7 and 9 fitted to the amplitude contour of data set B by solving the Yule-Walker equations. They 'explode' as all the fitted models are unstable. This is no surprise if one looks at the autocorrelation coefficients (figure 4.36, bottom). As mentioned in chapter 3.2.3 the autoregressive model fitted to a strictly periodical signal tend to be unstable.

Autoregressive models fitted to the amplitude contour of system C allow quite good predictions (cf. figure 4.39).

Figure 4.40 shows the amplitude contour of data set D, its autocorrelation function

[17]Note that the amplitude-axis has logarithmic scale. In normal plot the continuous parts cannot be seen at all.

[18]Amplitude modulation with a sine results in one sideband on the left and one on the right side of the peaks due to the main oscillation.

[19]This is equivalent to the fact that one could define three independent types of frequency modulations using maxima, minima or zero-crossings. The notion of modulations does not make sense for signals of arbitrary type, even if they are periodical.

and an AR-prediction that uses a model of order nine. The amplitude contour of data set D has an autocorrelation function that is falling faster so the quality of linear predictions is limited. Predictions using nonlinear models might give superior results in this case.

The method of delay coordinates was used to plot the phase portraits for the data sets B,C and D. The delay time used for this attractor reconstructions is ten times the sampling interval. The phase portrait of data set B (figure 4.44, top) shows the toroidal dynamics with a frequency ratio very close to eleven[20]. Two attractor reconstructions are shown for data set C. Figure 4.45 (top) was made from all data samples available[21], figure 4.45 (bottom) from about one fourth of the data set lying approximately in the middle of the time series. As the sampling rate is very close to an integer multiple[22] of the fastest oscillation a spurious structure occurs. A underestimation of the dimension of the attractor may appear if the computations are based on this part of the data. The phase portrait for data set D (figure 4.44, bottom) appears to be more diffuse.

The attractor dimensions for the global data sets C and D were estimated with the nearest neighbor procedure by E.J.Kostelich (the programs 'nn' and 'polyfit', cf. [50]). The dimension estimates obtained were $D \approx 2.2$ for data set C (cf. figure 4.2.2, top) $D \approx 2.4$ for data set C (cf. figure 4.2.2, bottom). The error of both values is about 0.15.

The Lyapunov exponents for data sets C and D were estimated with the programs 'eck' and 'expons' by E.J.Kostelich for various values for the embedding dimension, time delay and evolution time (cf. [50]). None of the obtained Lyapunov exponents is zero, as expected for stationary dynamics[23]. The obtained sets of Lyapunov exponents even lead to Kaplan-Yorke dimensions smaller than two. Therefore they must be considered as spurious values. The reason that the estimation of the Lyapunov exponents fails may lie in the fact that the data is not transient free, which will be seen in the next section.

[20] One can count the eleven passes of the trajectory near the upper right corner of the plot.
[21] except the samples from the transient phase.
[22] The ratio is almost exactly 57.
[23] Corresponding to a perturbation in the direction of the trajectory.

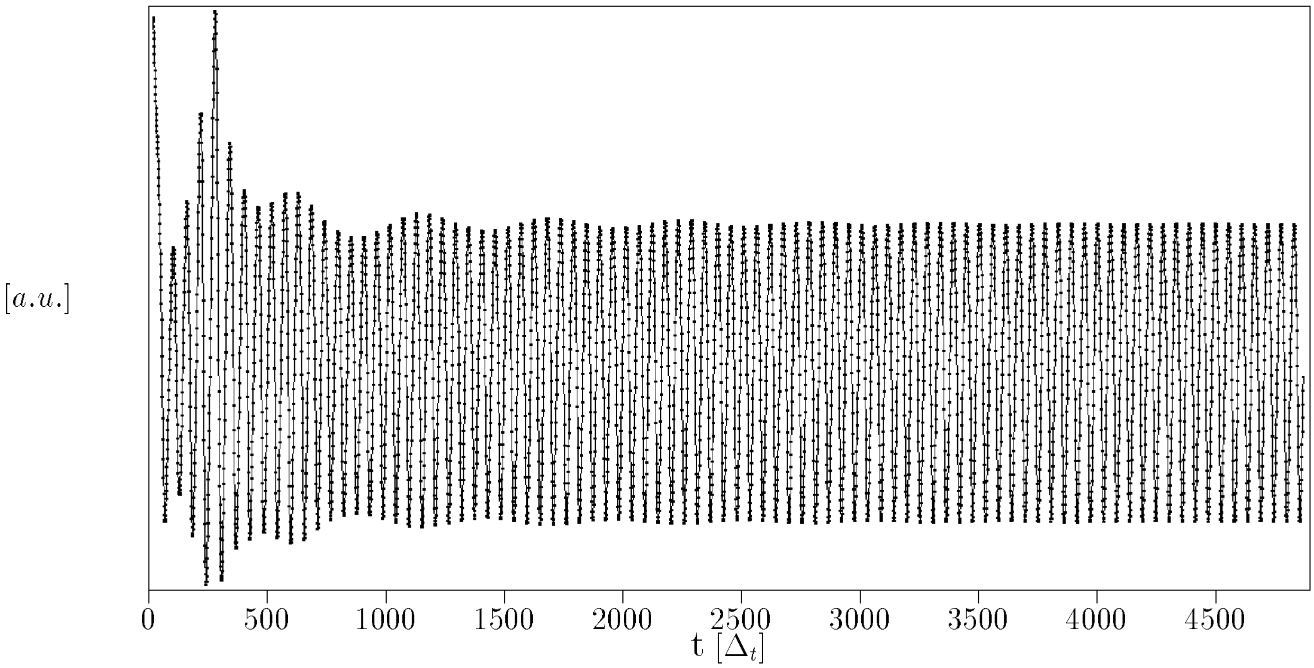

Figure 4.24: **Temporal profile of the global data set A including transient.**
The plotted quantity is the partial pressure of carbon monoxide.

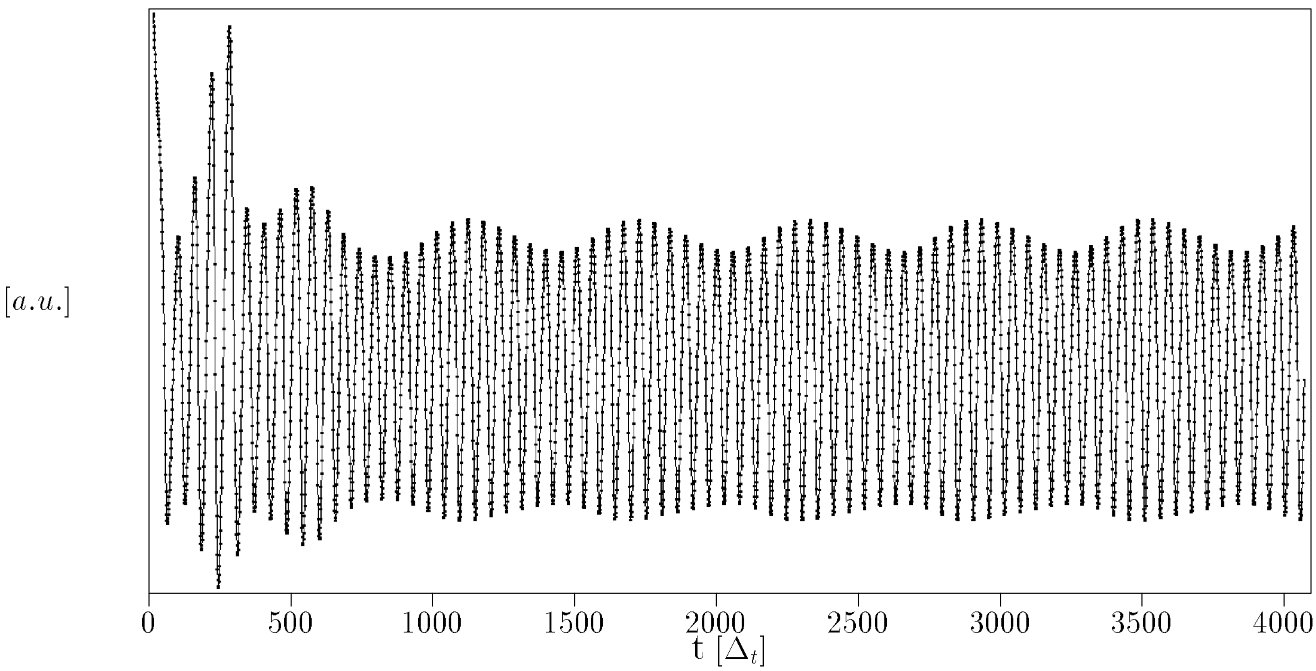

Figure 4.25: **Temporal profile of the global data set B including transient.**
The plotted quantity is the partial pressure of carbon monoxide.

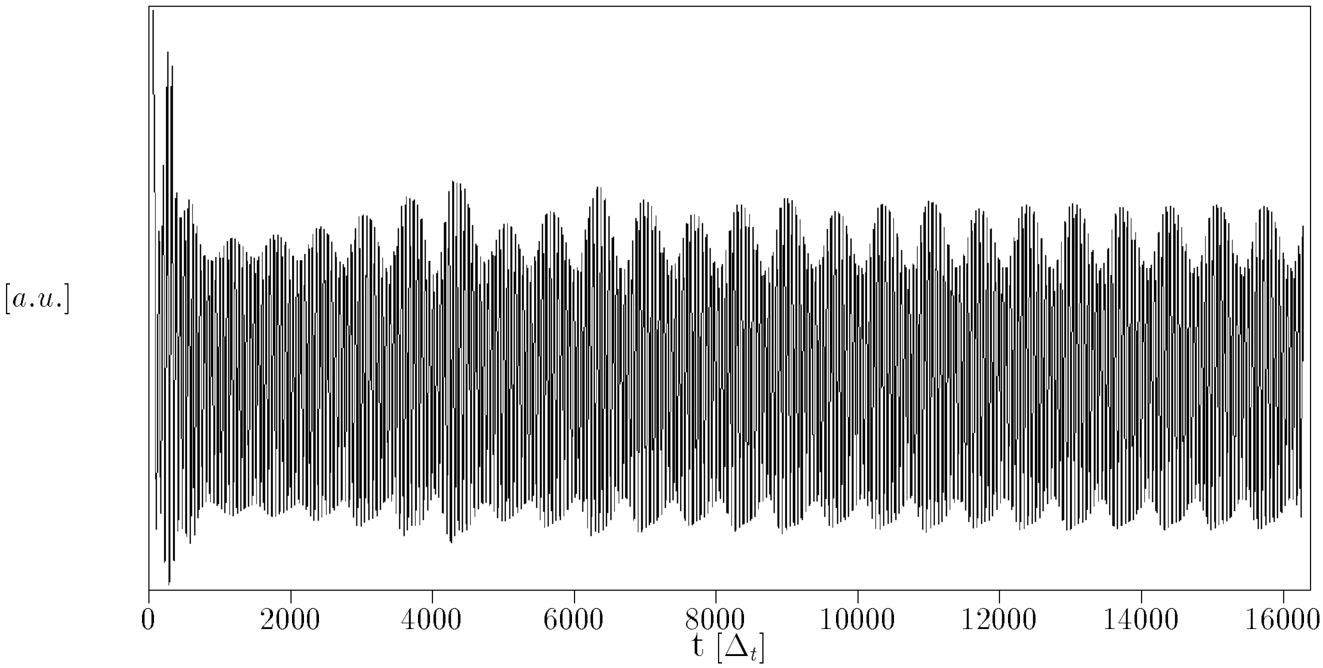

Figure 4.26: **Temporal profile of the global data set C including transient.** *The plotted quantity is the partial pressure of carbon monoxide.*

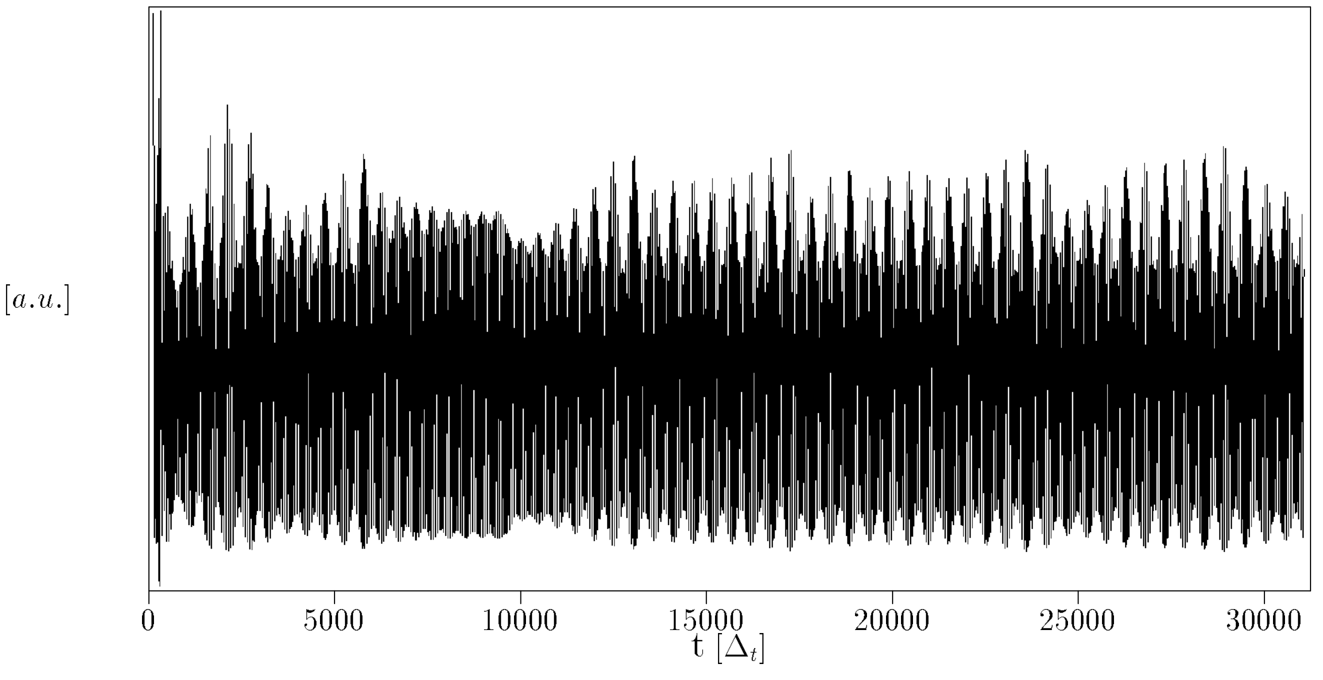

Figure 4.27: **Temporal profile of the global data set D including transient.** *The plotted quantity is the partial pressure of carbon monoxide.*

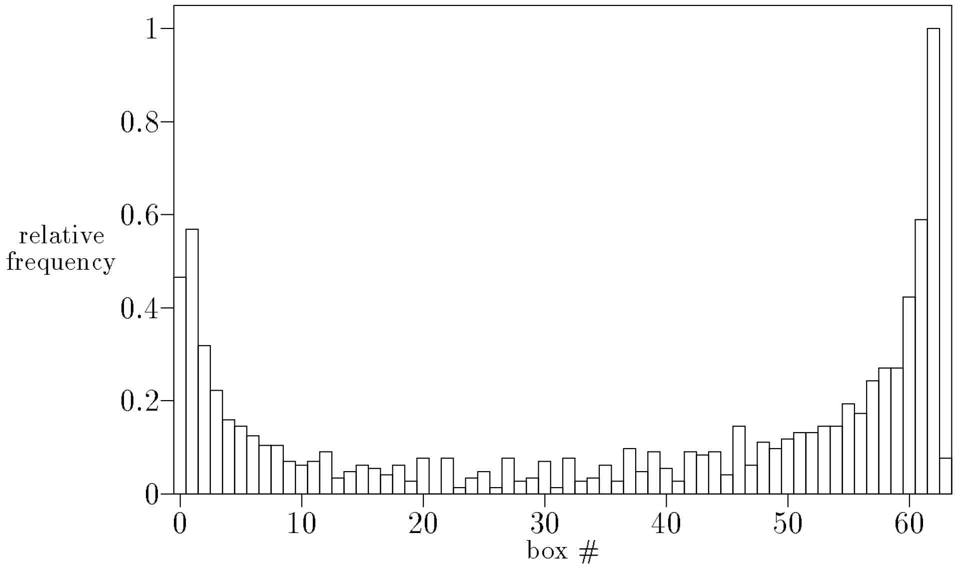

Figure 4.28: **Histogram for the global data set A.**
This is a distribution statistics about the time series. The total range of all values of the time series is divided into 64 'boxes'. For each box the occurrence of time series values falling into it is counted. The values are normalized to make the greatest relative frequency equal to one.

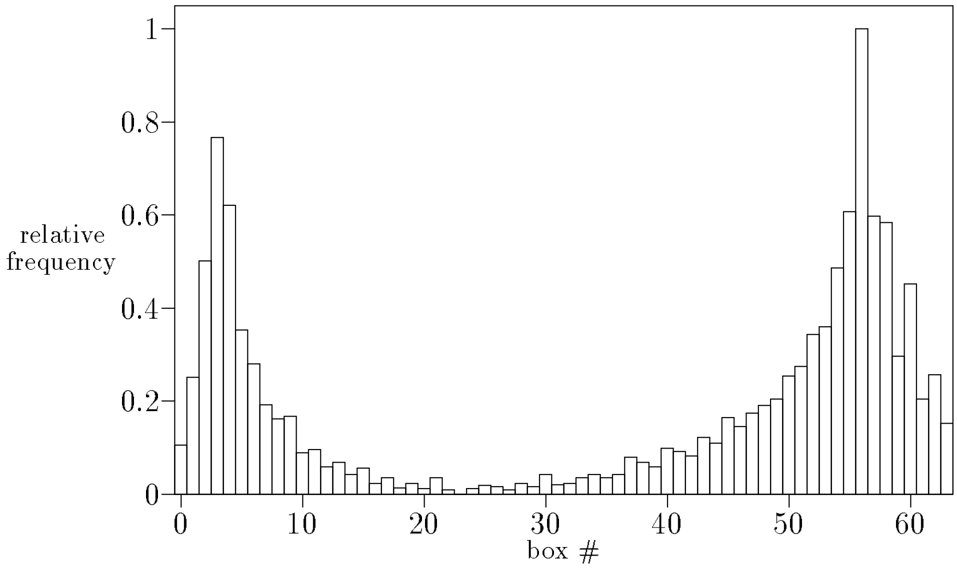

Figure 4.29: **Histogram for the global data set B.**

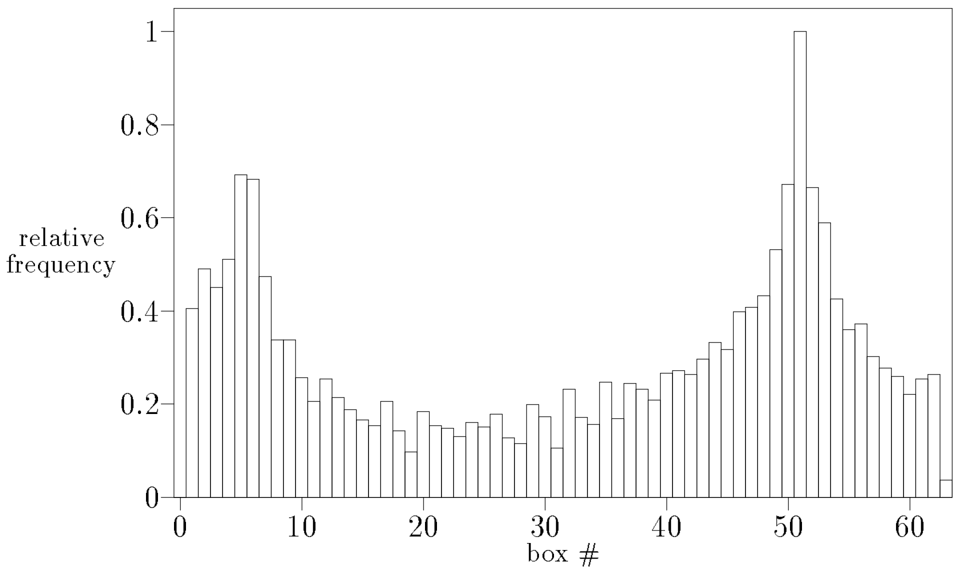

Figure 4.30: **Histogram for the global data set C.**

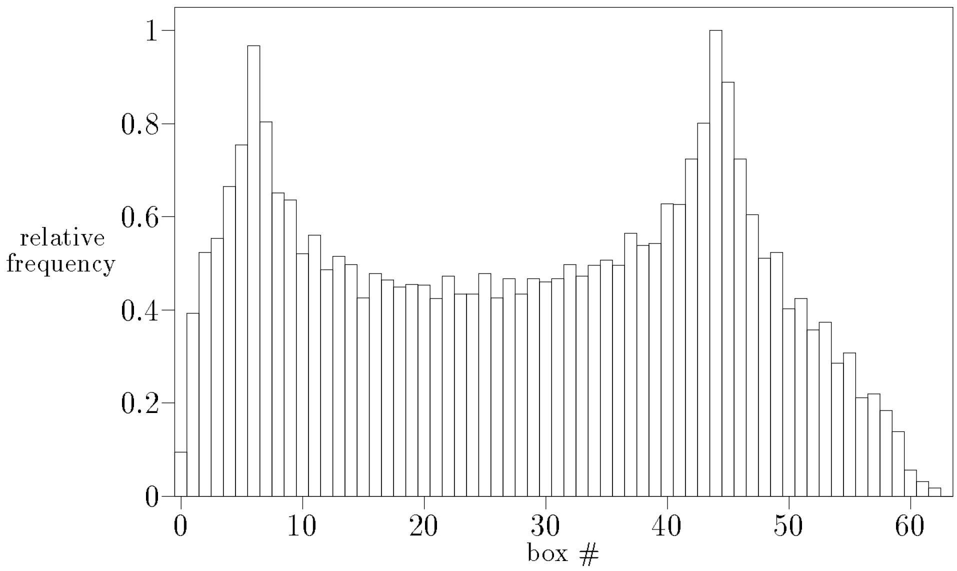

Figure 4.31: **Histogram for the global data set D.**

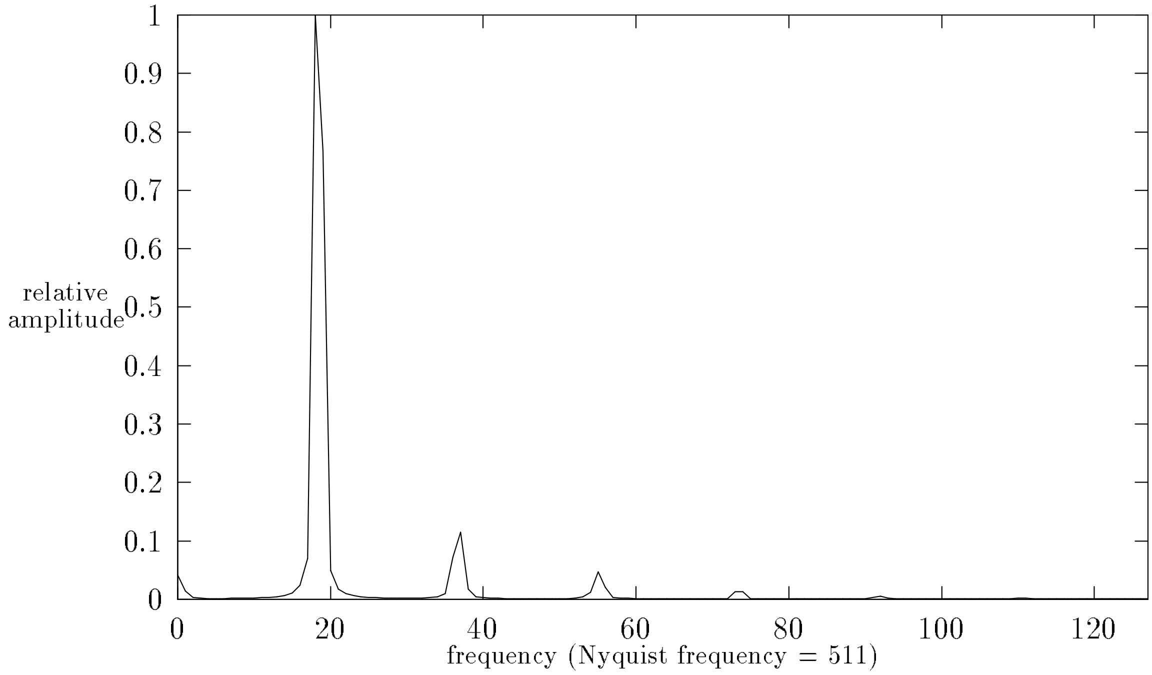

Figure 4.32: **Spectrum of the global data for A, the periodic case.**
The maximum frequency shown is 1/4·Nyquist frequency.

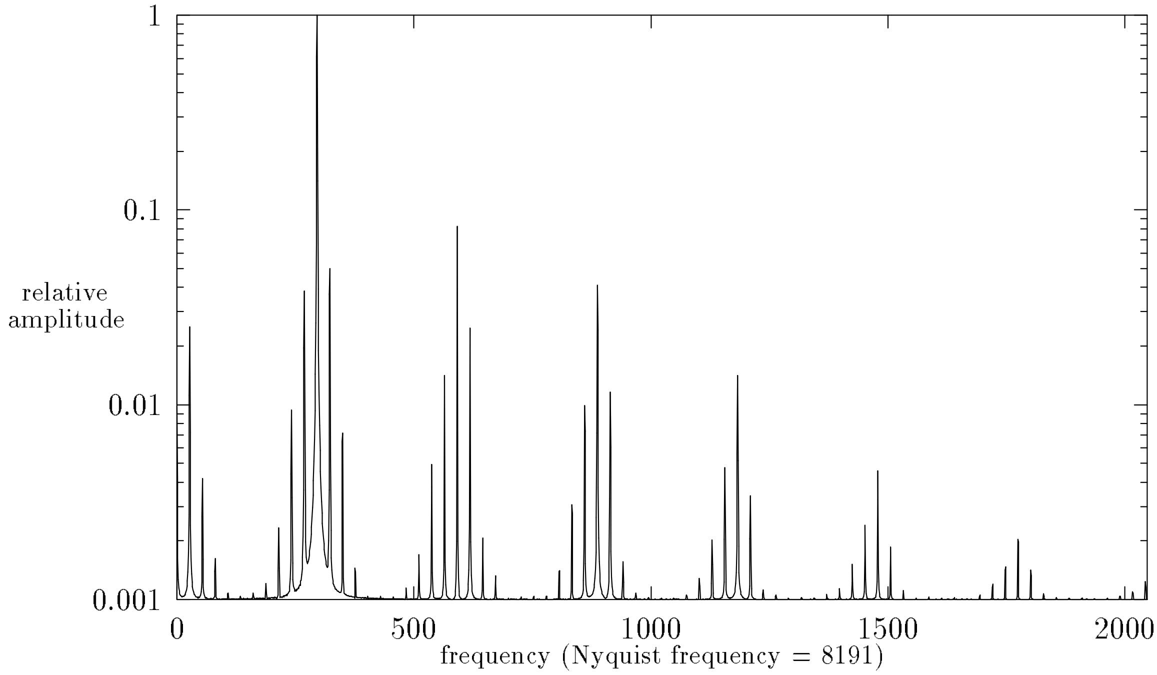

Figure 4.33: **Spectrum of the global data for B, the toroidal case.**
The maximum frequency shown is 1/4·Nyquist frequency. Note the logarithmic scale.

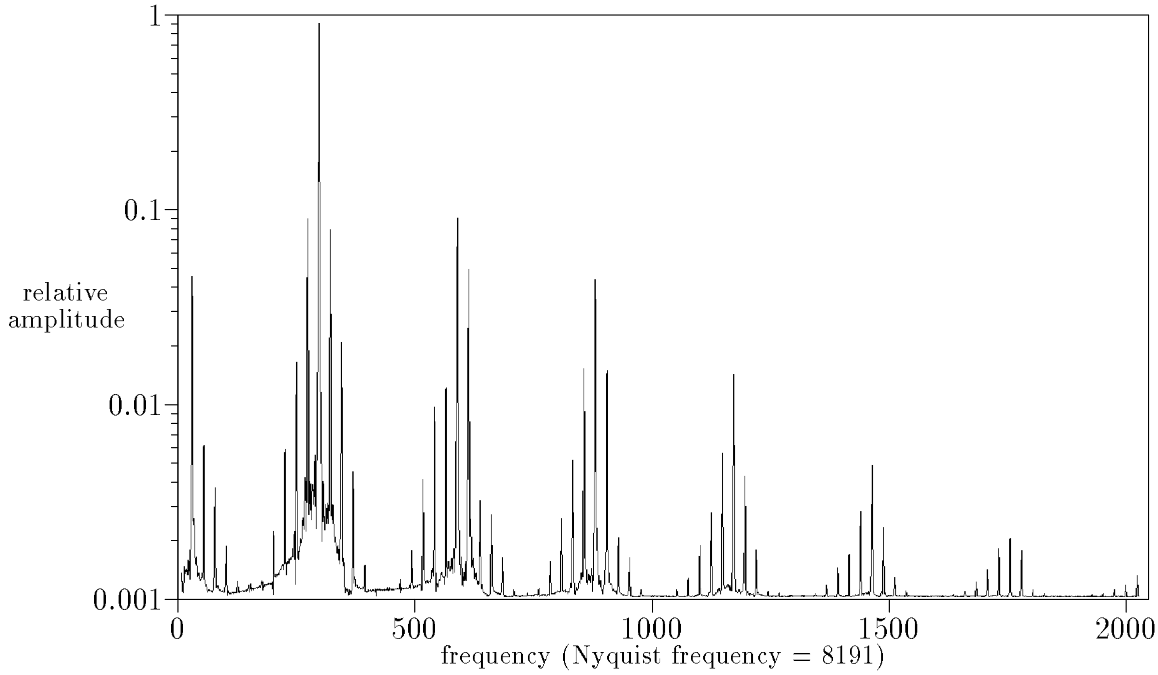

Figure 4.34: **Spectrum of the global data for C, the case of temporal chaos.** *The maximum frequency shown is* 1/4·*Nyquist frequency. Note the logarithmic scale.*

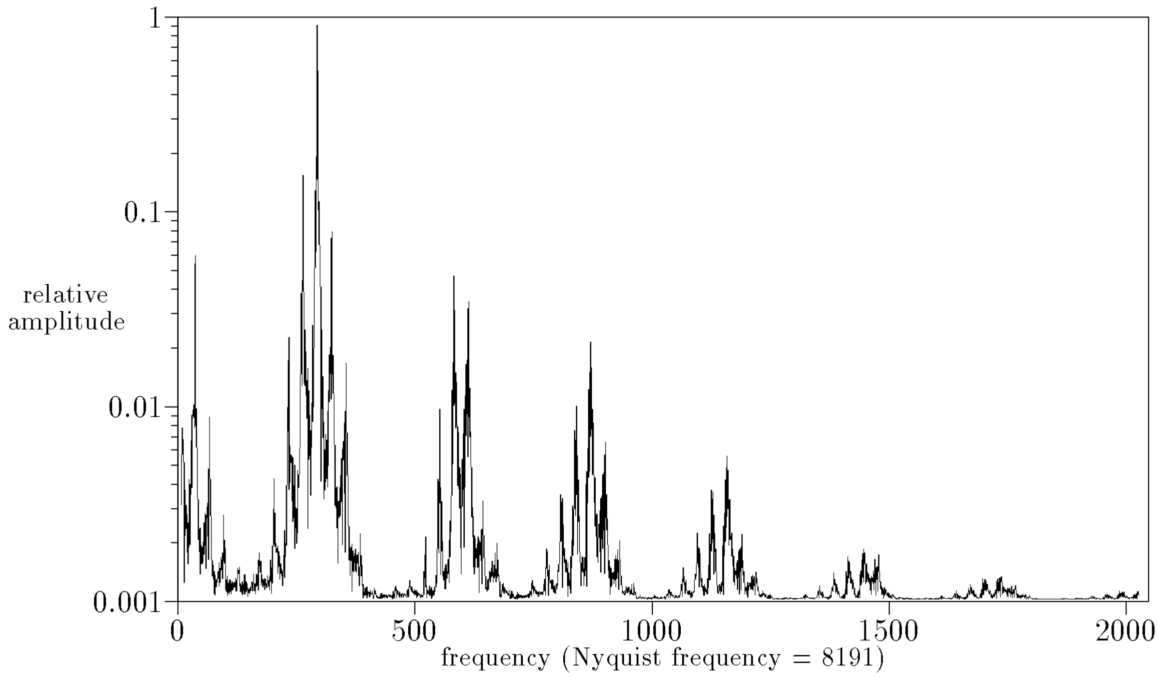

Figure 4.35: **Spectrum of the global data for D, the case of weak turbulence.** *The maximum frequency shown is* 1/4·*Nyquist frequency. Note the logarithmic scale.*

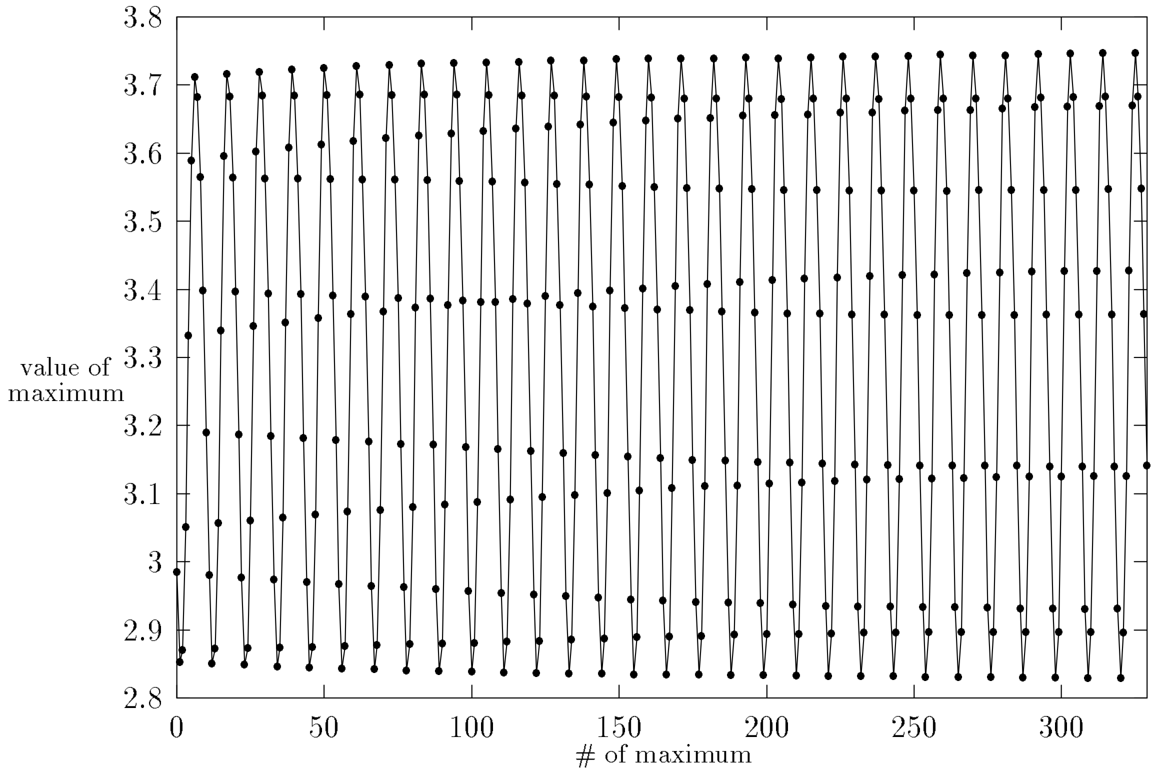

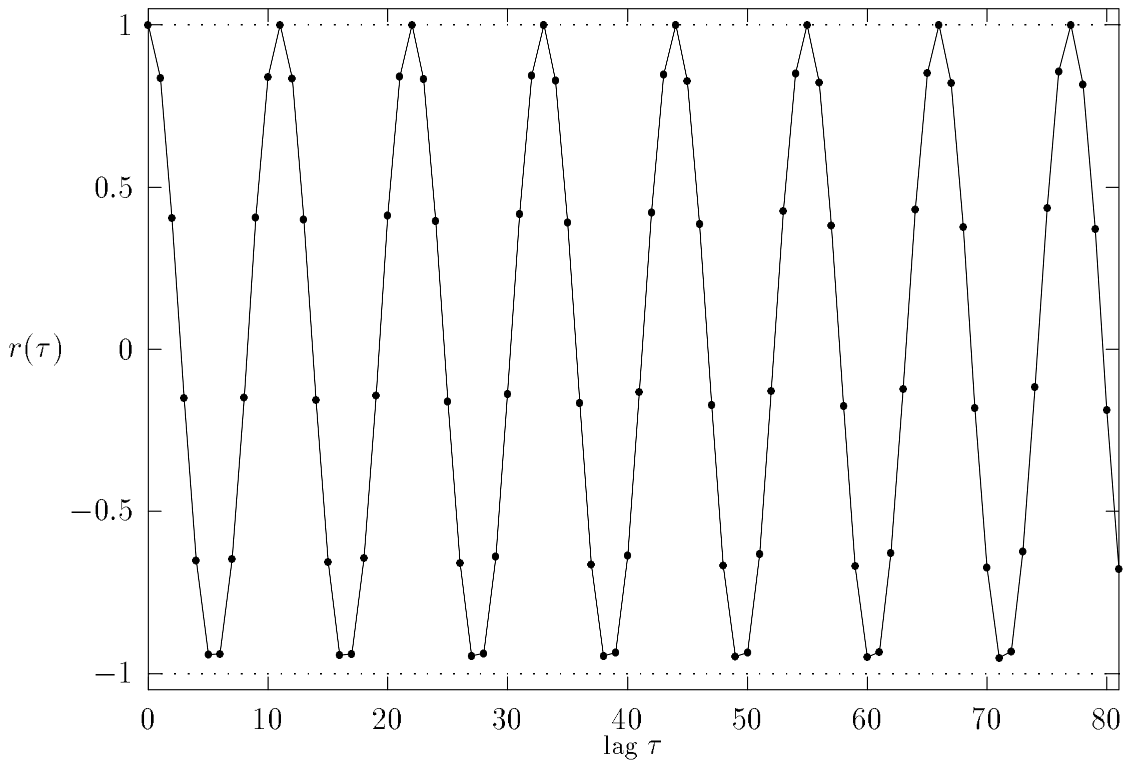

Figure 4.36: **The amplitude contour (top) and its autocorrelation coefficients for the global data for system B.**

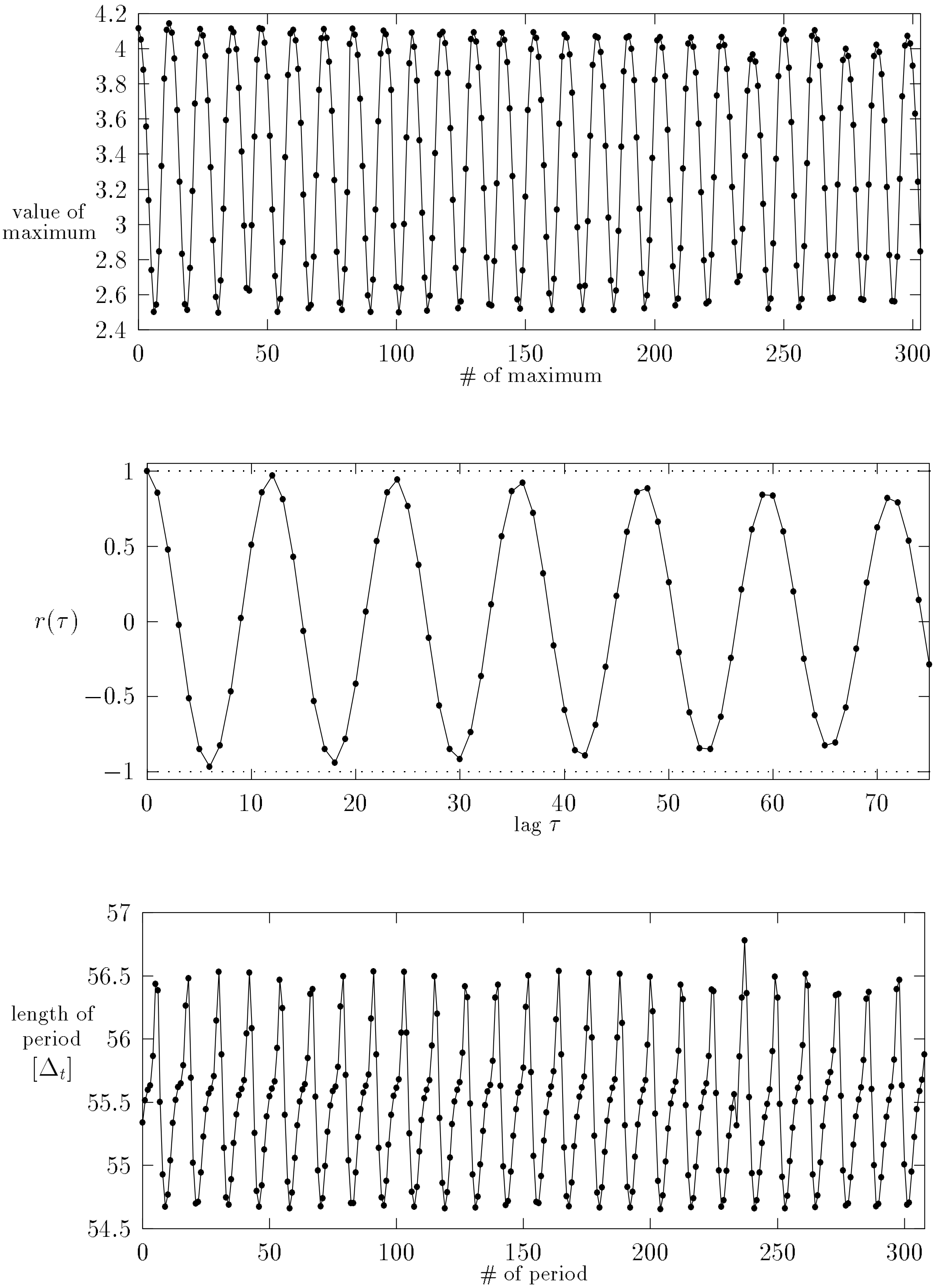

Figure 4.37: **The amplitude contour (top), its autocorrelation coefficients and the period contour for the global data for system C.**
The modulation depth is 20% *for the amplitude modulation and approximately* 2% *for the frequency modulation.*

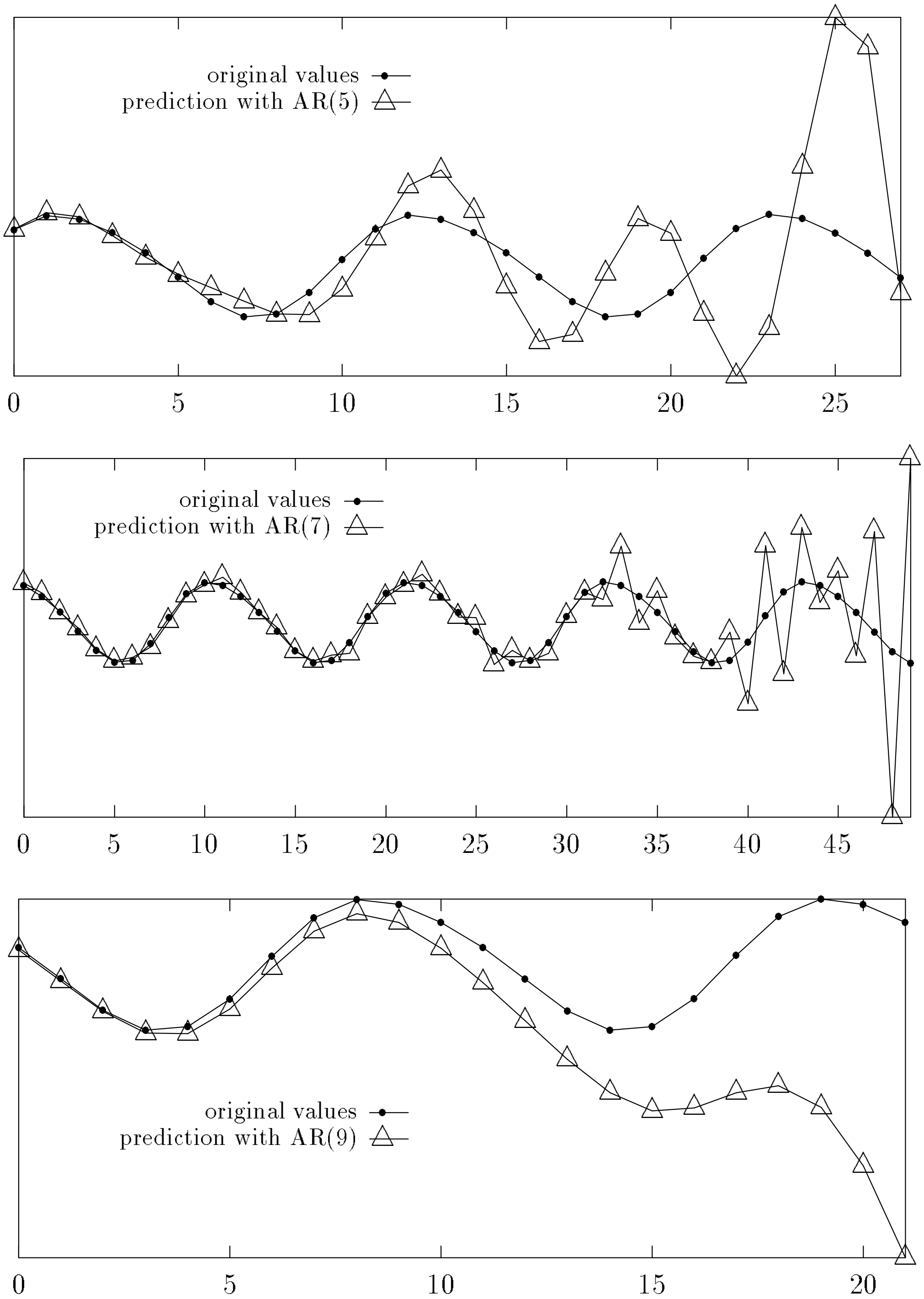

Figure 4.38: **Predictions using autoregressive models for the amplitude contour of the global data set B.**
The data is the sequence of the interpolated maxima of the global data for system B. Its autocorrelation function oscillates undamped (cf. figure 4.38). It is usual that the models fitted to strictly periodical data are unstable which leads to the typical 'exploding' realizations shown here. Models of greater order will not help, a relocation of the zeros of the characteristic equation seems to be the only solution here.

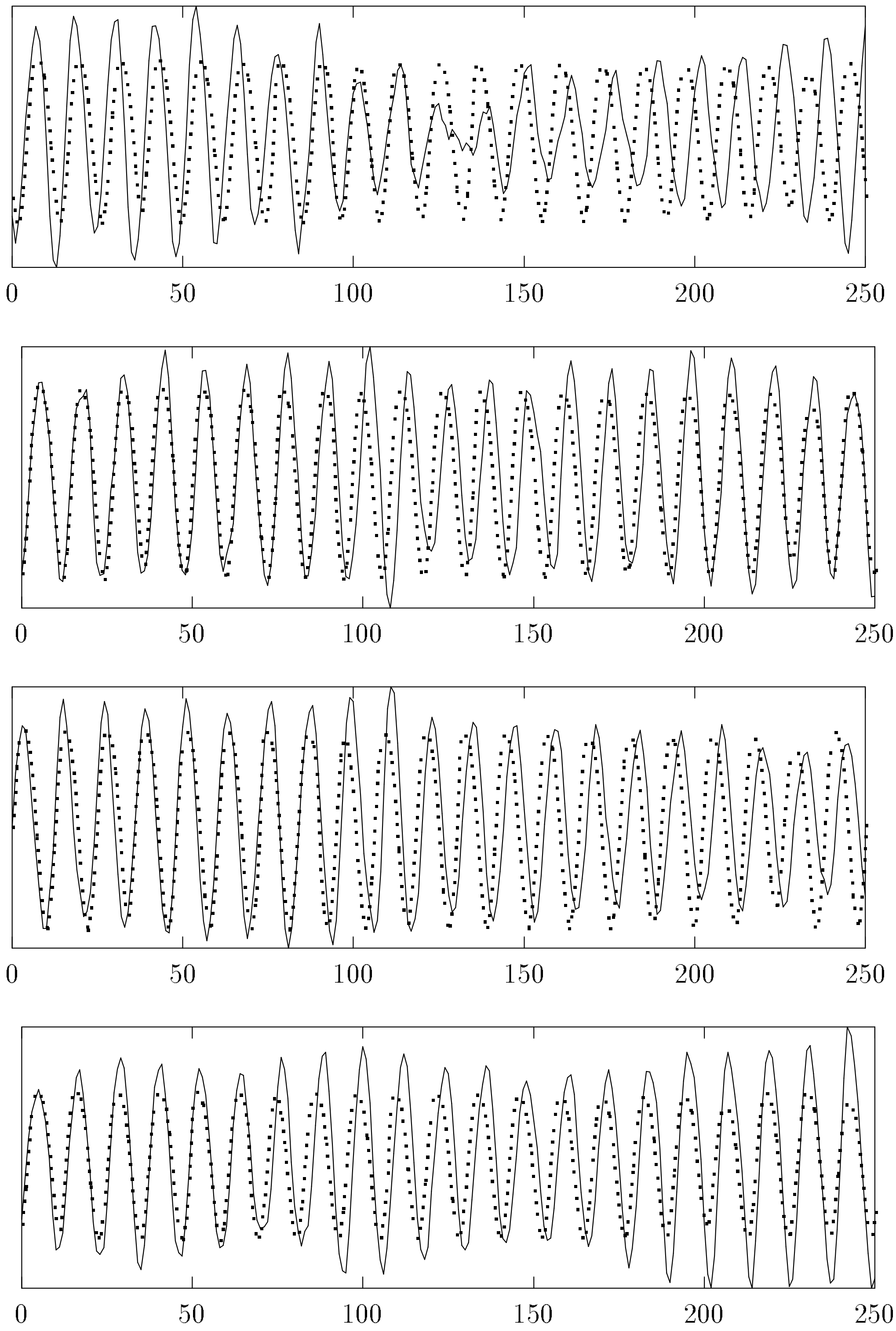

Figure 4.39: **Predictions using autoregressive models of orders 5,7,9 and 32 for the amplitude contour of the global data set C.**
Dotted lines are the plots of the original data, the sequence of the interpolated maxima of the global data for system C. The autocorrelation function falls only slowly (cf. figure 4.39). There is some optimal value for the order of the model (here about $p = 9$*), a greater value (cf. lowest plot) does not improve the results.*

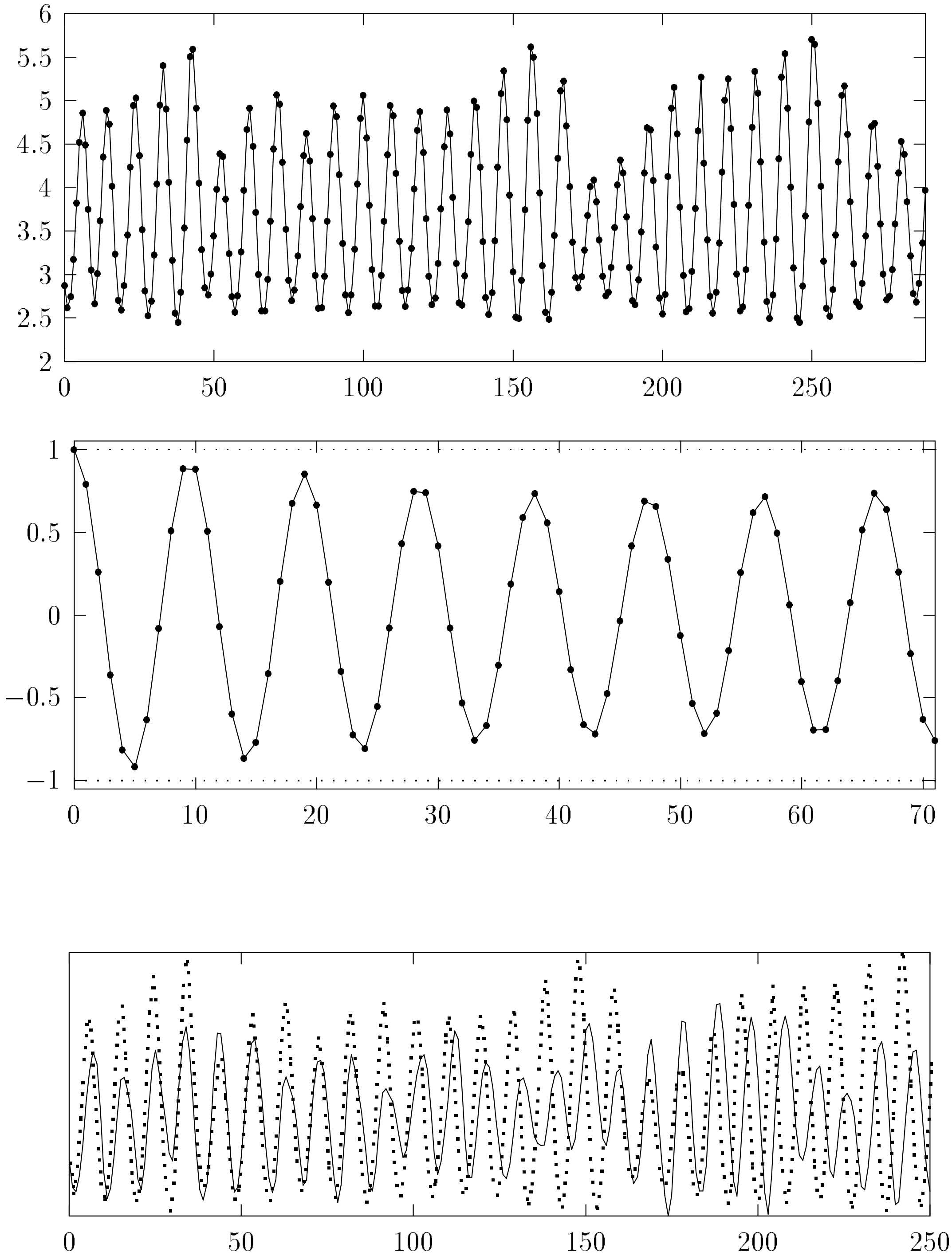

Figure 4.40: **Amplitude contour of the global data set D (top), its autocorrelation function and a prediction using an autoregressive model of order 9 (bottom).**
The amplitude contour is the sequence of the interpolated maxima. In the lower plot the original data corresponds to the dotted line.

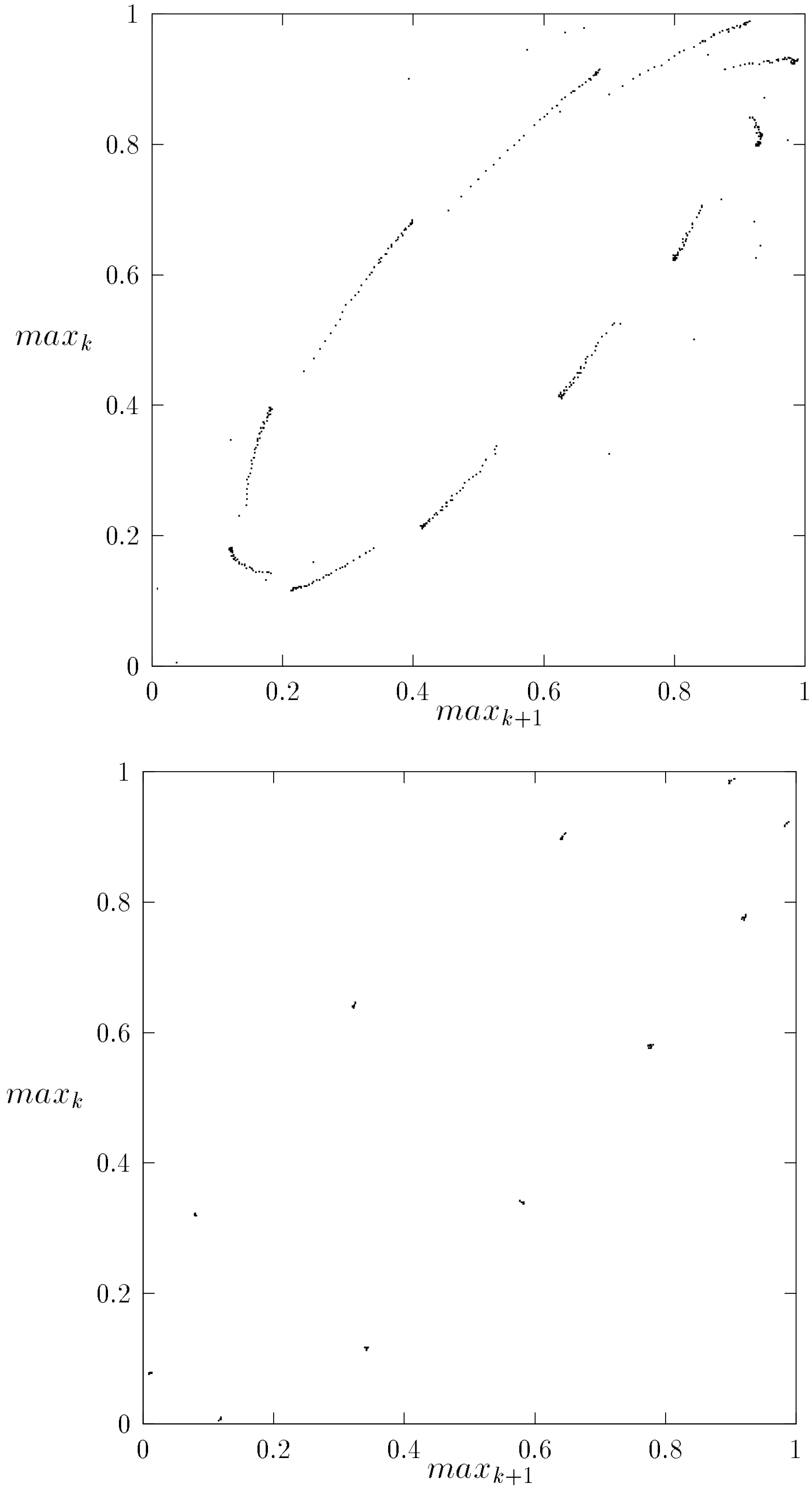

Figure 4.41: **Maximum map of data set B.**
Top: Maximum map of the data including transient part. Points belonging to earlier times lie in the less dense parts. Bottom: Maximum map of the last eight beat periods. For both plots non-interpolated maxima were used.

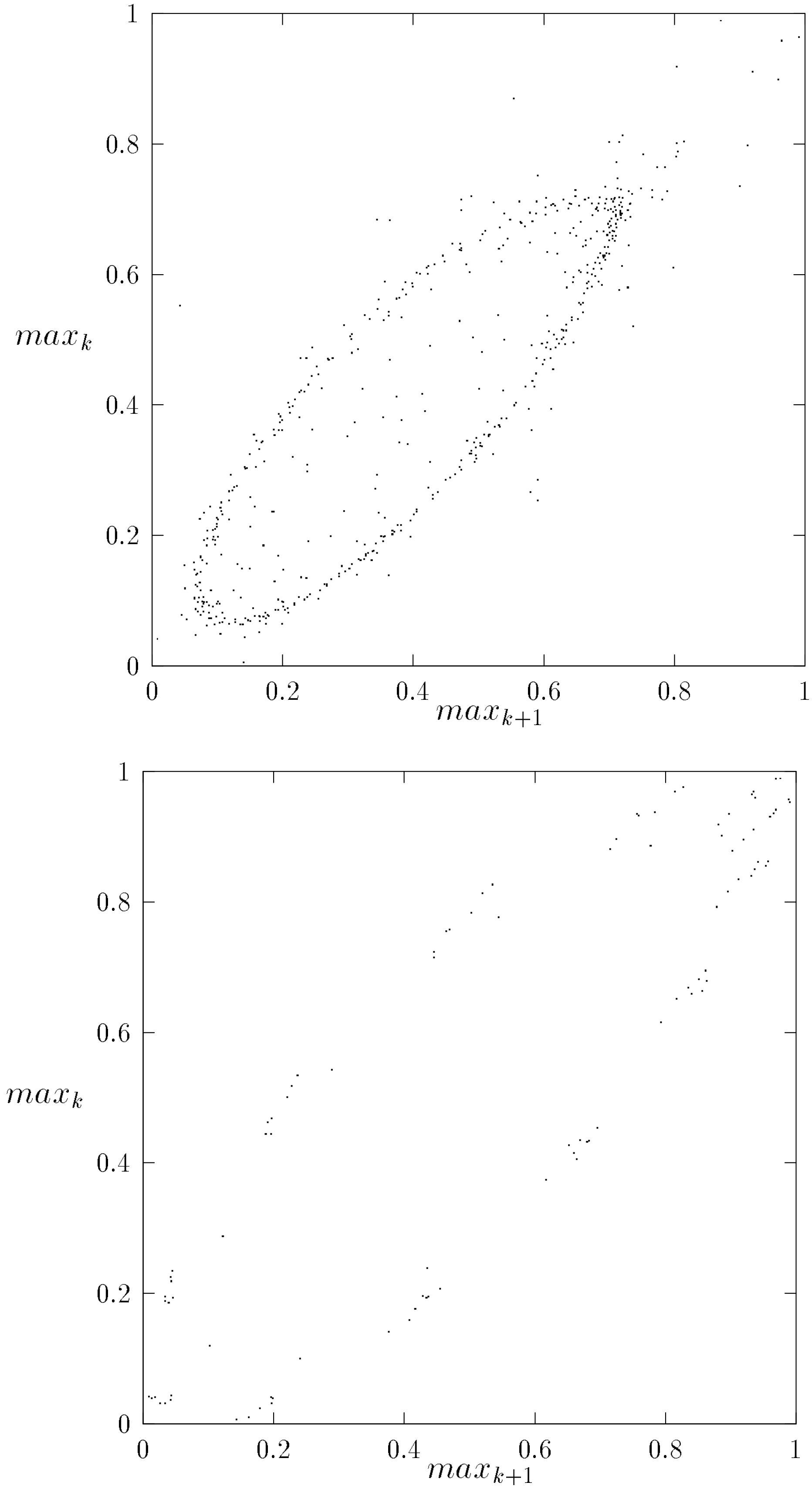

Figure 4.42: **Maximum map of data set C.**
Top: Maximum map of the data including transient part. Bottom: Maximum map of the last eight beat periods. For both plots non-interpolated maxima were used.

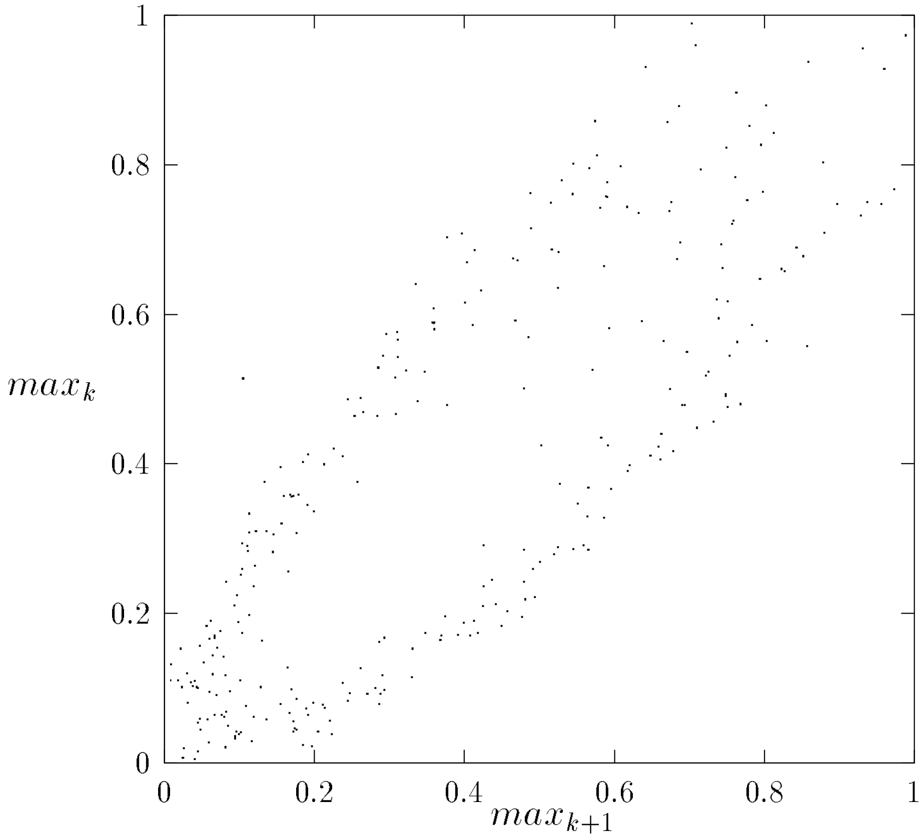

Figure 4.43: **Maximum map of data set D.**
Non-interpolated maxima were used for this plot.

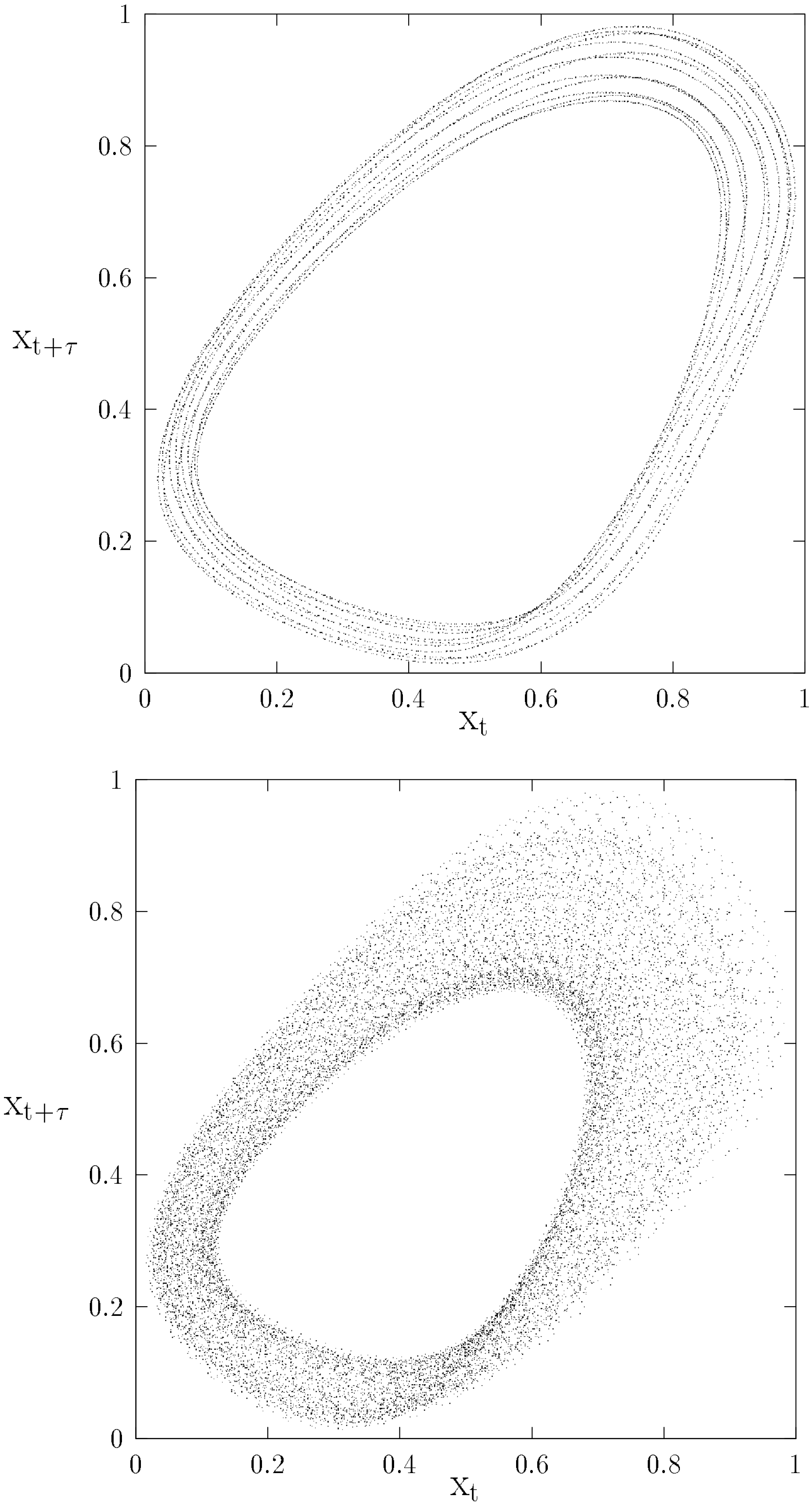

Figure 4.44: **Phase portrait of data sets B (top) and D (bottom).** *The delay time* τ *is* $10 \cdot \Delta_t$.

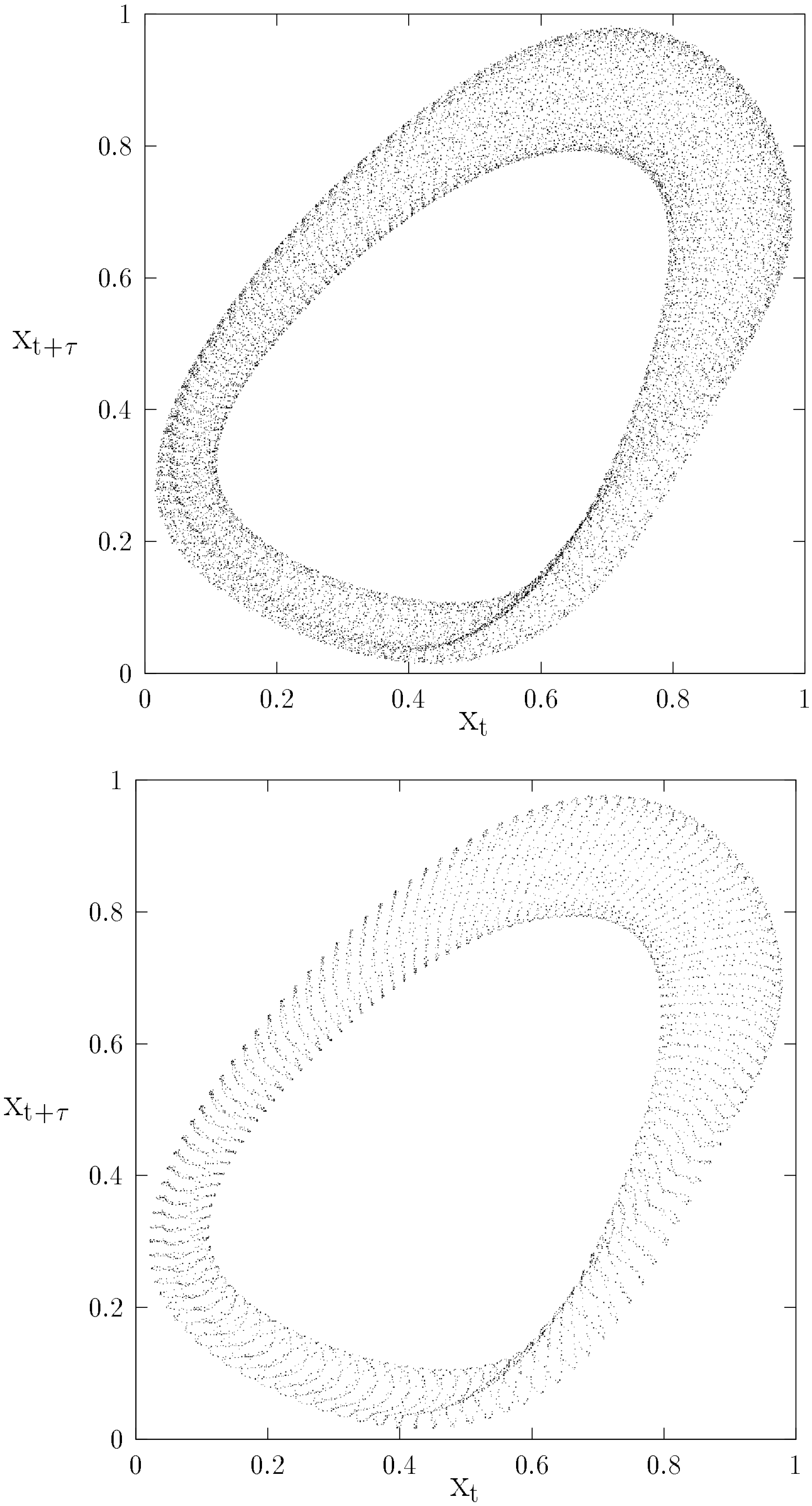

Figure 4.45: **Phase portraits of data set C.** *The delay time* τ *is* $10 \cdot \Delta_t$. *The lower plot shows a phase portrait of of the samples 6500...10500 (of total 17200 values). The sampling rate is very close to a integer multiple of the fastest oscillation. The resulting attractor reconstruction might suggest a false type of dynamics.*

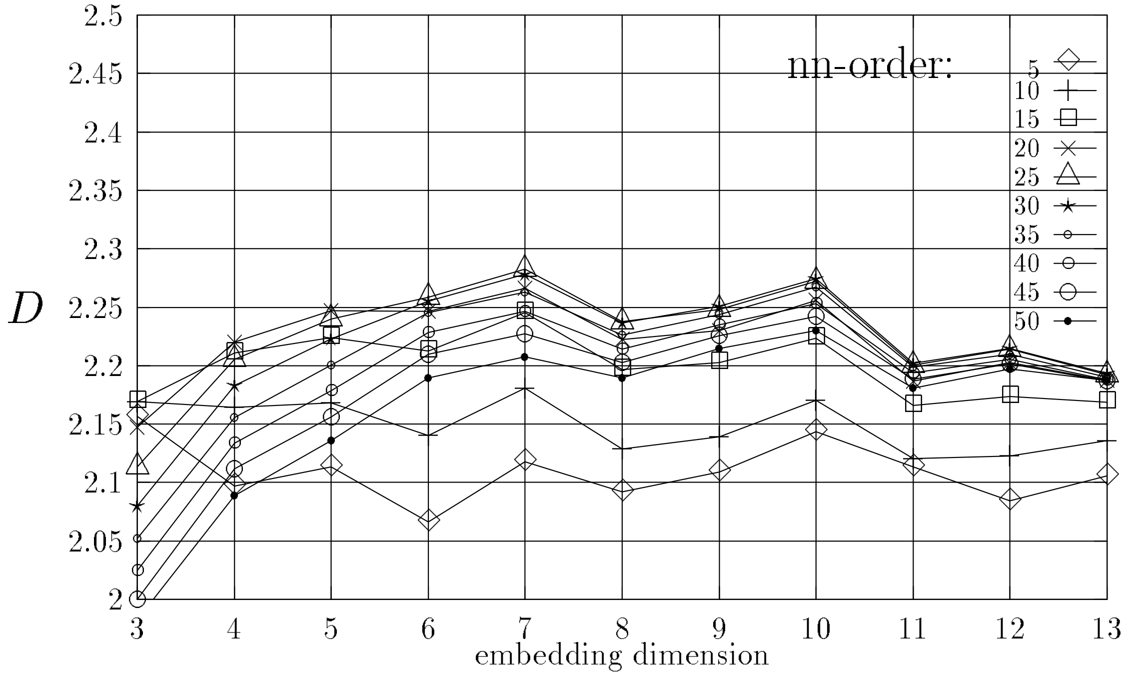

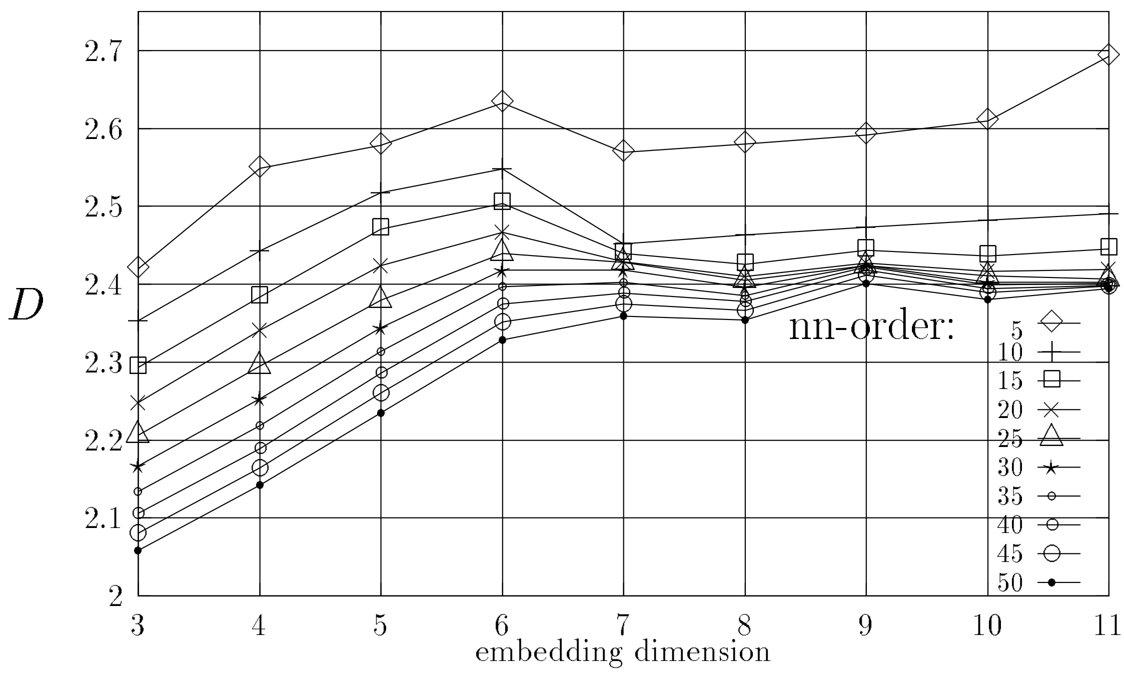

Figure 4.46: **Dimension estimates for the global data sets C (top) and D (bottom).**
The dalay time used is $\tau = 10 \cdot \Delta_t$.

4.2.3 Analysis of the Spatio-Temporal Data

A plot of the spatio-temporal dynamics for data set D is shown in figure 4.47. In the darker stripes one can recognize the modulation of the signal. The modulation period is about eleven times longer than the period of the dominating oscillation. Spatio-temporal plots of the data sets A...C look very similar, except that there is no modulation for data set A. The shape of the waves can be seen in figure 4.48 which is a detail of the same simulation. Here twice the spatial sampling rate and four times the temporal sampling rate was used compared to data set D.

The empirical modes for the data sets A,B,C,D were computed using the singular value decomposition. The table of the singular values (table 4.4) shows that for A and B a few modes dominate. More than 99% of the (standard deviation of the) dynamics is contained within the first six modes, see table 4.5. For systems with both temporal and spatial regular behavior this distribution is not surprising. For data set C the first six modes describe only about 91.5% of the dynamics and one would need already the first 14 modes to cover more than 99%. This may be seen as a hint that the dynamics of C is not purely the case of temporal chaos, any fluctuations of the locations of the patterns will lead to a slower decay of the singular values. Finally for data set D the singular values decrease slower than for the other cases. It shows a weakly turbulent dynamics, the borders of the typical structures slightly fluctuate. Due to the nature of the POD one cannot expect to find a few dominating modes (cf. chapter 3.5.2). The distribution of the singular values for the data sets A - D is shown in figure 4.49, note the logarithmic vertical scale.

In the first empirical modes for data set B (see figure 4.51) the shape of the characteristic patterns of the corresponding data can easily be recognized. The higher modes (i.e. those corresponding to small singular values) must not be interpreted as a pattern found by the POD, their shapes are rather determined by the orthogonality property for the empirical modes: They generally tend to become more oscillatory in the regions of the borders between the patterns.

The 'x-shaped' amplitude of the fifth empirical mode of data set C (see figures 4.53 and 4.55) looks very different from mode amplitudes 1...4 . Such x-shaped mode amplitudes were found several times when a POD was performed on different data sets. It was investigated whether this special shape is an artefact of the algorithm, the implementation used or whether it gives 'real information' about the data. First it was ruled out that this is an effect of the specific implementation of the POD. For that purpose the spatio-temporal data was cut into blocks of equal length in time. The blocks were swapped and the resulting data set was used as a test input for the POD. A flaw in the implementation should have been detected if the new mode amplitude was of a similar shape than the original one. The resulting mode, however, was exactly what is predicted by the definition of the POD (cf. figures 4.56 and 4.58): As it is insensitive to a permutation of the photos, the POD of any permutation of the input photos should lead to a result with the same modes and corresponding amplitudes which are permutated in the same way as the photos were. This indeed was the form of the output obtained, the implementation of the SVD[24] seems to be as reliable as its authors state.

It could be suspected that such a mode amplitude is either caused by a remaining transient in the data or that it is an effect caused by some property of the singular value decomposition. For data without transient[25] such x-shaped amplitudes did never occur. This is a strong hint that empirical modes with such amplitudes should be considered as effects of transients in the data. The specific forms of the mode amplitudes are due to the orthogonality property of the amplitudes from a POD: Even if only a part of data set B is used as input for the POD then the mode amplitude describing the transient always keeps its x-shaped form (cf. figure 4.57). The POD adjusts the form of the modes in a way that the amplitudes describing transients always seem to suffer a phase rotation of 180 degrees. Using short parts of a data set tends to shifts the number of the first x-shaped mode amplitude towards higher values. This can be expected because shorter data sets only contain a smaller portion of transient behavior. The corresponding singular values give an estimate of the percentage of transient behavior.

Among the mode amplitudes of data set D (figure 4.54) there are also 'irregular' ones (namely number 4,6 and 9), which also seem to suffer a phase rotation. But their form is not due to transients, they reflect the fluctuation of the borders of the stripe patterns in the data. Again the corresponding singular values give a certain measure for the amount of turbulent behavior. The modes then indicate where the turbulence occurs.

This means that the POD can supply valuable information for data sets where it strictly spoken must not be applied. If the transient or turbulent behavior of a system is not too strong the POD produces modes that can be assigned to that parts of the dynamics. These modes and their amplitudes indicate where and when that behavior occurs, the singular values give a measure for its strength.

The empirical modes for the simulations with differrent parameters cannot be compared to each other because of the periodic boundary conditions that lead to a different distribution of the stripe patterns for each parameter value.

For linear systems there is a one to one relation between the eigenmodes and the frequencies of the system. This statement does not hold for nonlinear systems. However, a certain correspondence between the frequencies of the system and the empirical modes can be observed here. The lower frequency of the torus can clearly be found as a modulation in mode amplitude number two in figure 4.53 whereas in amplitude one it seems to be absent. Here the modes one and two describe the dynamics in the two different types of spatial stripes in the data, very similar to figure 4.47 the modulation mainly takes place in one of the two types.

[24]Which is a C-routine taken from [3].

[25]several synthetic data sets and the data sets E and F analized in chapter 4.1.

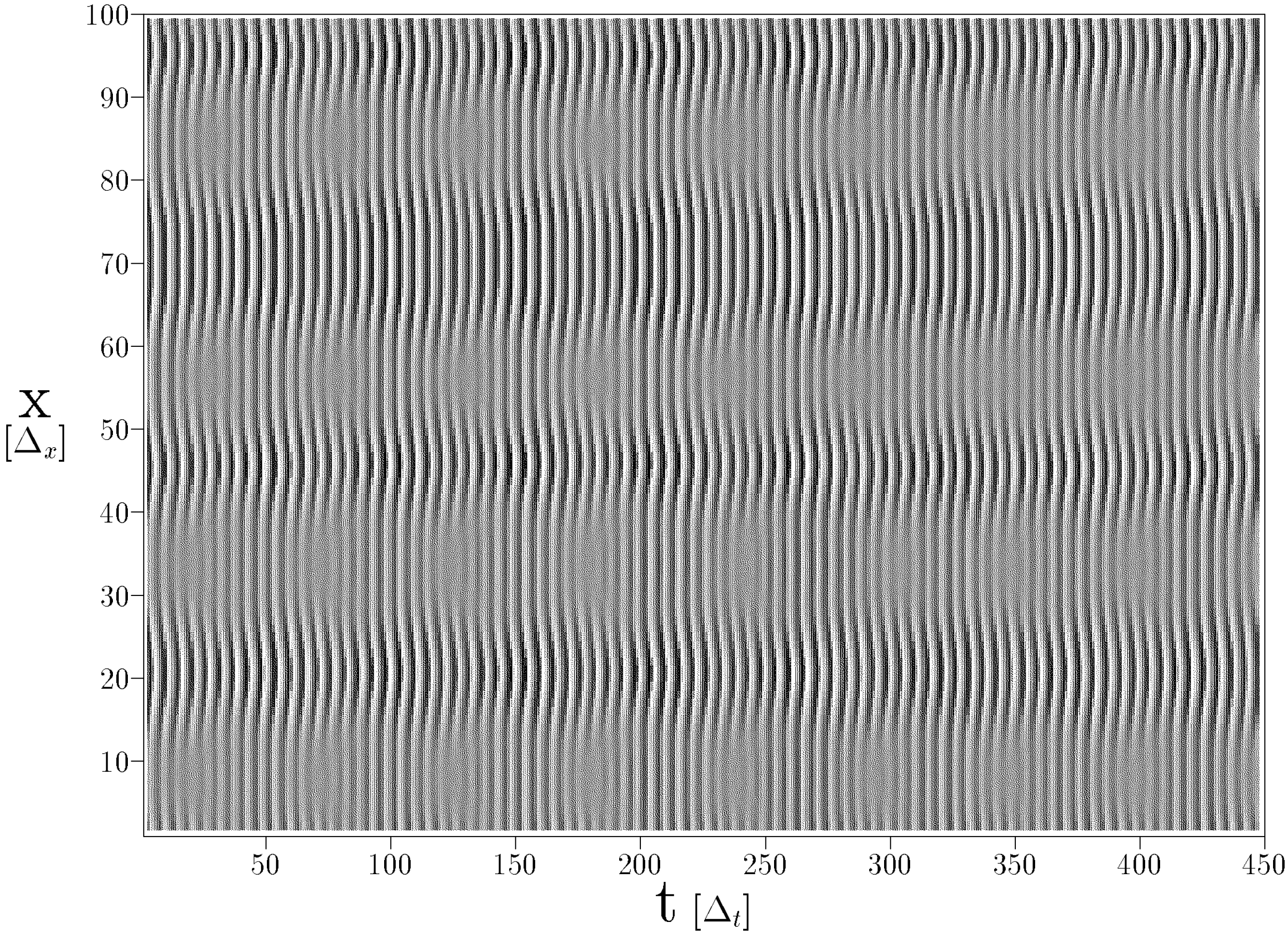

Figure 4.47: **Spatio-temporal plot of data set D.**
Dark regions correspond to high partial pressures of carbon monoxide.

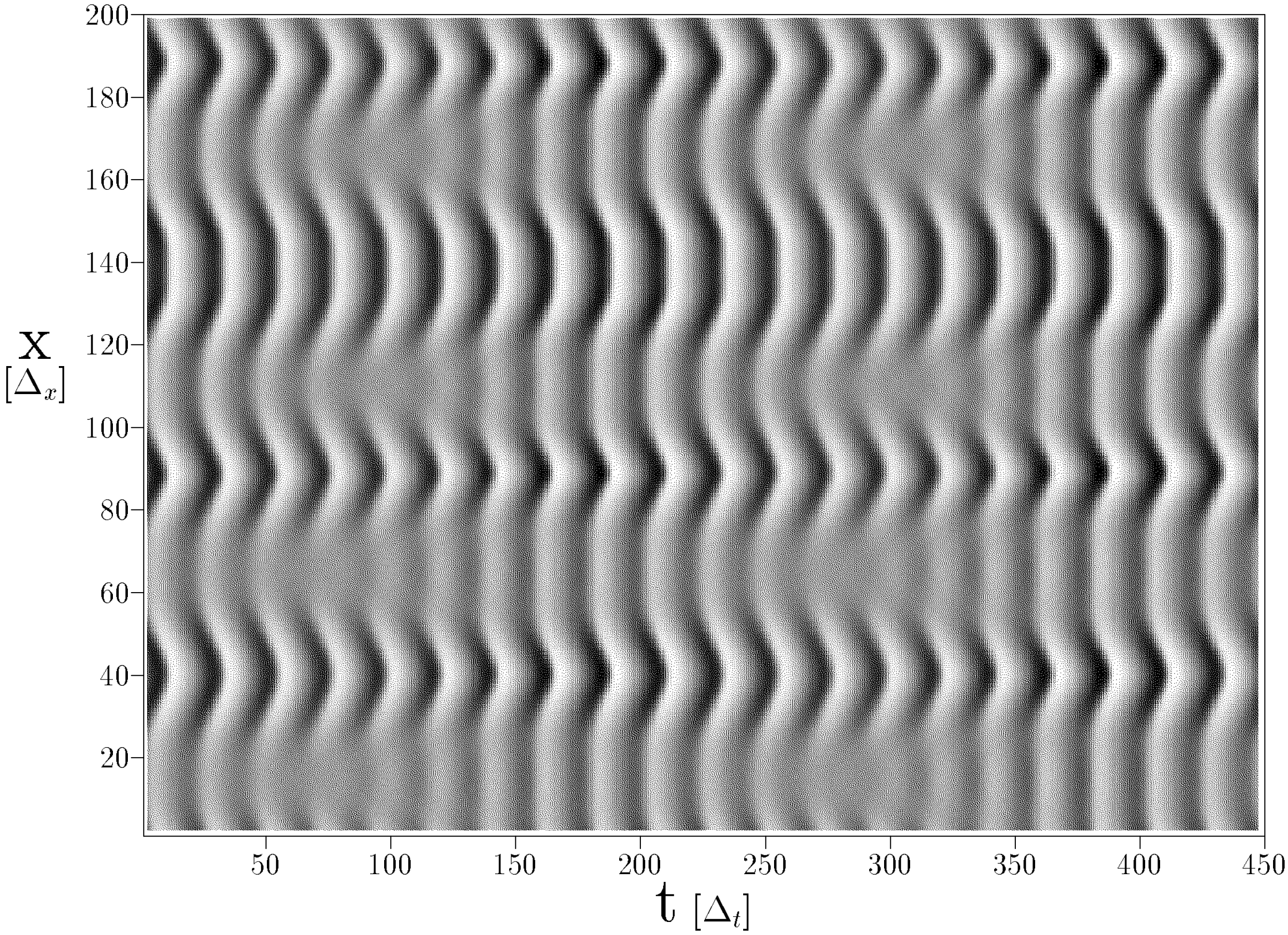

Figure 4.48: **Detail of data set D.**
These data were recorded with a higher sampling-rate and at more locations than the data used for the analysis in this thesis.

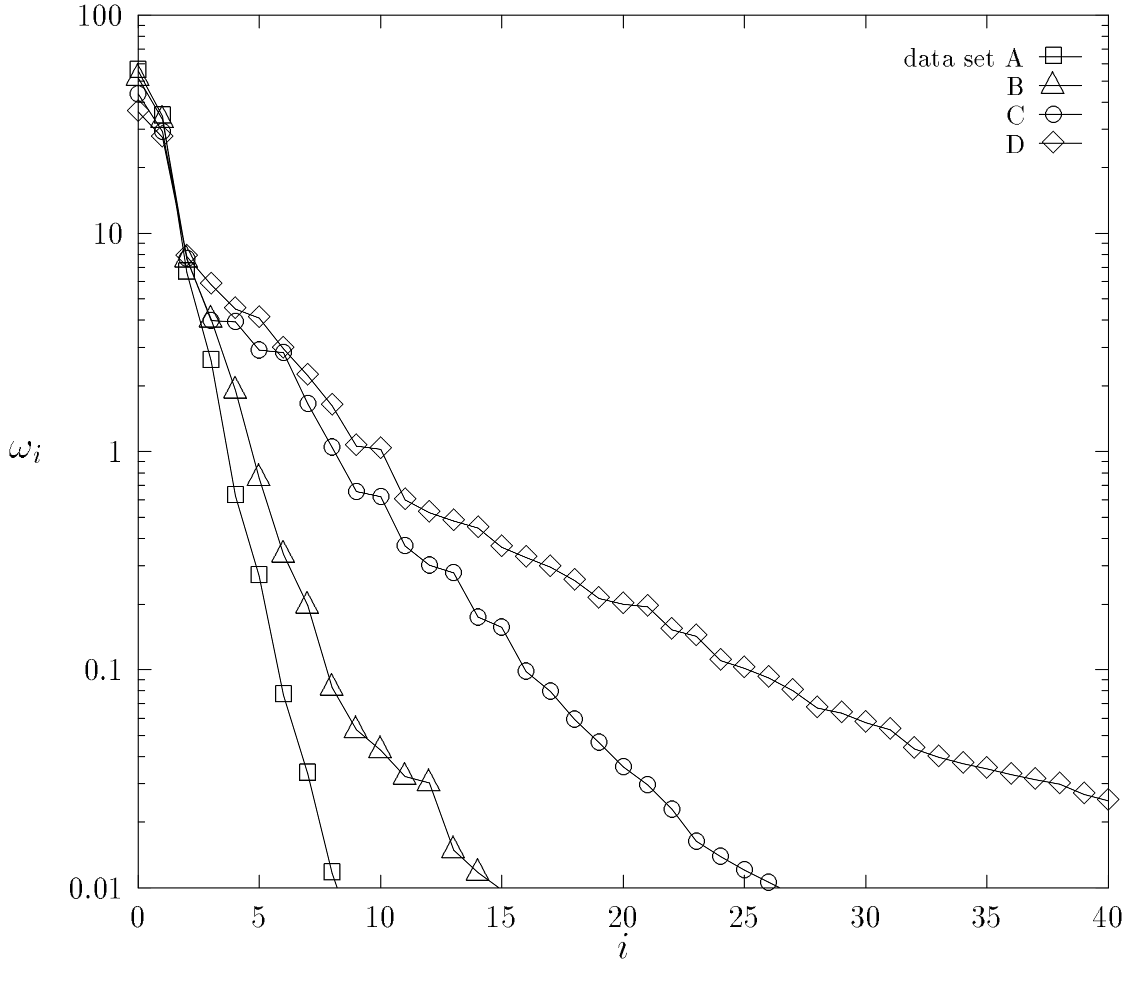

Figure 4.49: **Logarithmic plot of the first 20 singular values for A - D.** *The singular values are plotted versus the number of their corresponding empirical modes.*

#	A: periodic	B: torus	C: temporal chaos	D: weak turbulence
1	55.47424	51.72563	43.57567	35.9689
2	34.27286	33.14202	29.31886	27.5575
3	6.609278	7.599817	7.684667	7.82502
4	2.607328	4.024955	3.989968	5.80164
5	0.623500	1.905375	3.925190	4.50114
6	0.268399	0.755899	2.918001	4.09786
7	0.076638	0.337746	2.849799	2.95492
8	0.033294	0.197319	1.650753	2.22570
9	0.011695	0.082795	1.042468	1.61913
10	0.005611	0.053195	0.655008	1.05982

Table 4.4: **List of the first ten singular values for data sets A - D.**
They are normalized to sum up to 100%. Each value tells how much of the standard deviation of the original data is described by the corresponding empirical mode.

#	A: periodic	B: torus	C: temporal chaos	D: weak turbulence
1	55.47424	51.72563	43.57567	35.9689
2	89.74710	84.86766	72.89454	63.5264
3	96.35638	92.46748	80.57921	71.3514
4	98.96371	96.49243	84.56917	77.1531
5	99.58721	98.39781	88.49436	81.6542
6	99.85561	99.15371	91.41237	85.7521
7	99.93224	99.49145	94.26216	88.7070
8	99.96554	99.68877	95.91292	90.9327
9	99.97723	99.77157	96.95539	92.5518
10	99.98285	99.82476	97.61040	93.6117

Table 4.5: **The first ten cumulative singular values for data sets A - D.**
The value at number k tells how much of the standard deviation of the original data is described by the all empirical modes up to mode number k.

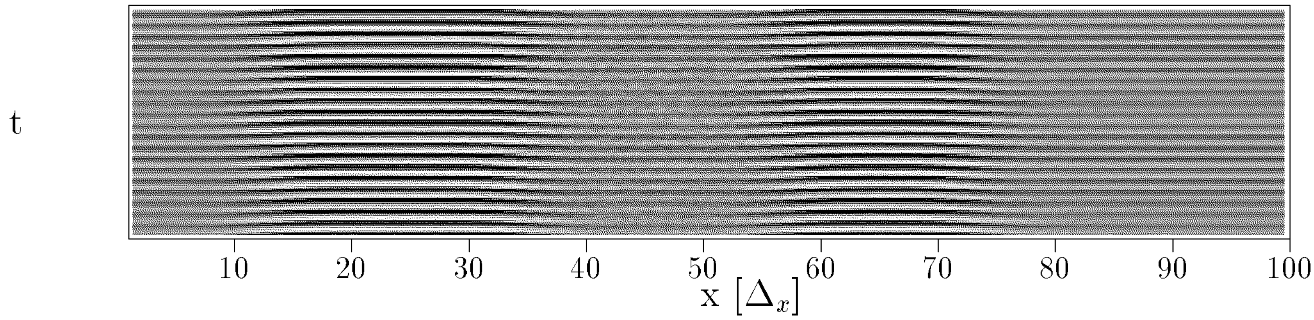

Figure 4.50: **Detail of spatio-temporal data set B, cf. figure below.**

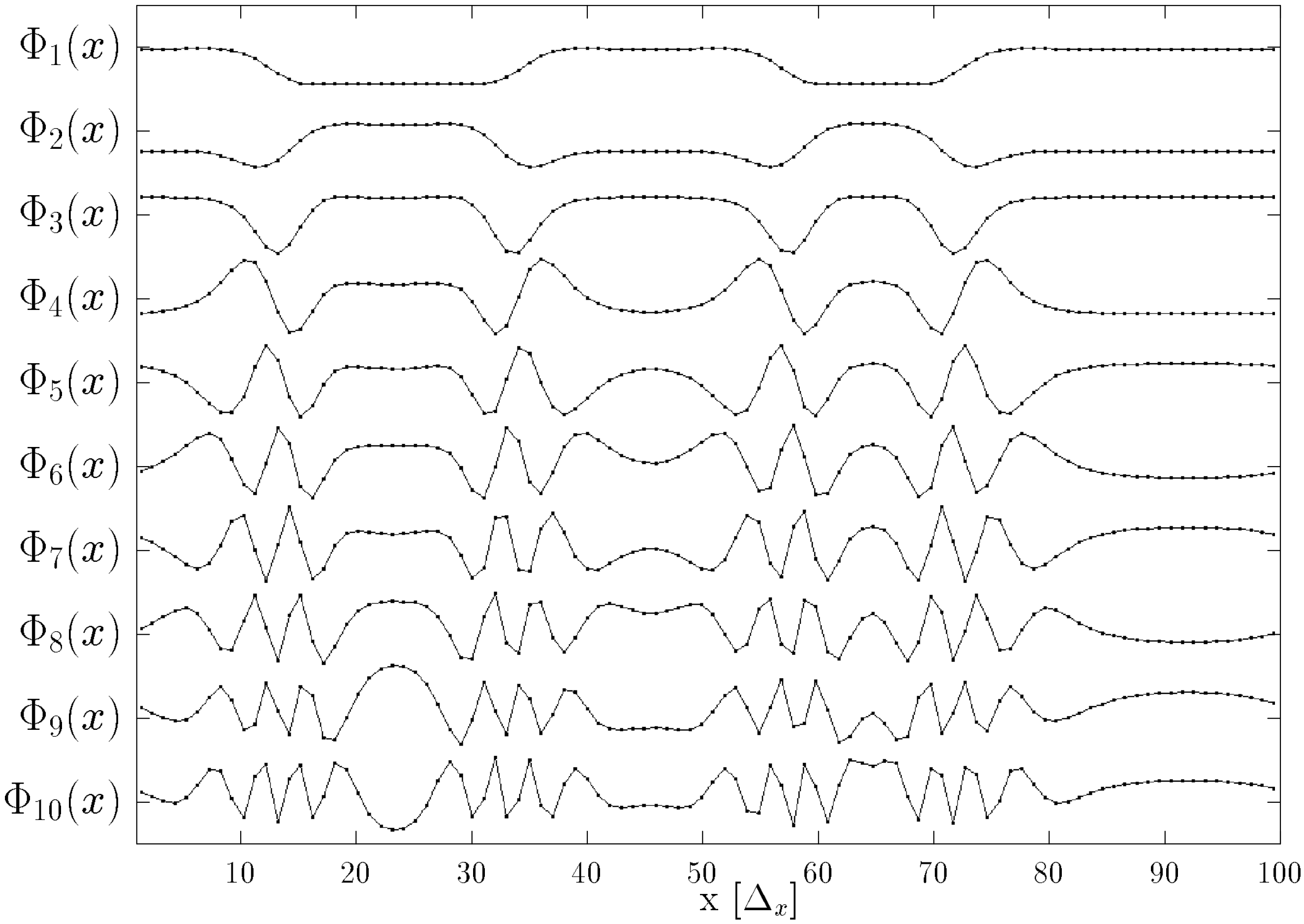

Figure 4.51: **The first ten empirical modes $\Phi_k(x)$ for data set B.**
Compare with above figure to see how the modes correspond to the spatial pattern of the data. Each mode is a vector of norm one.

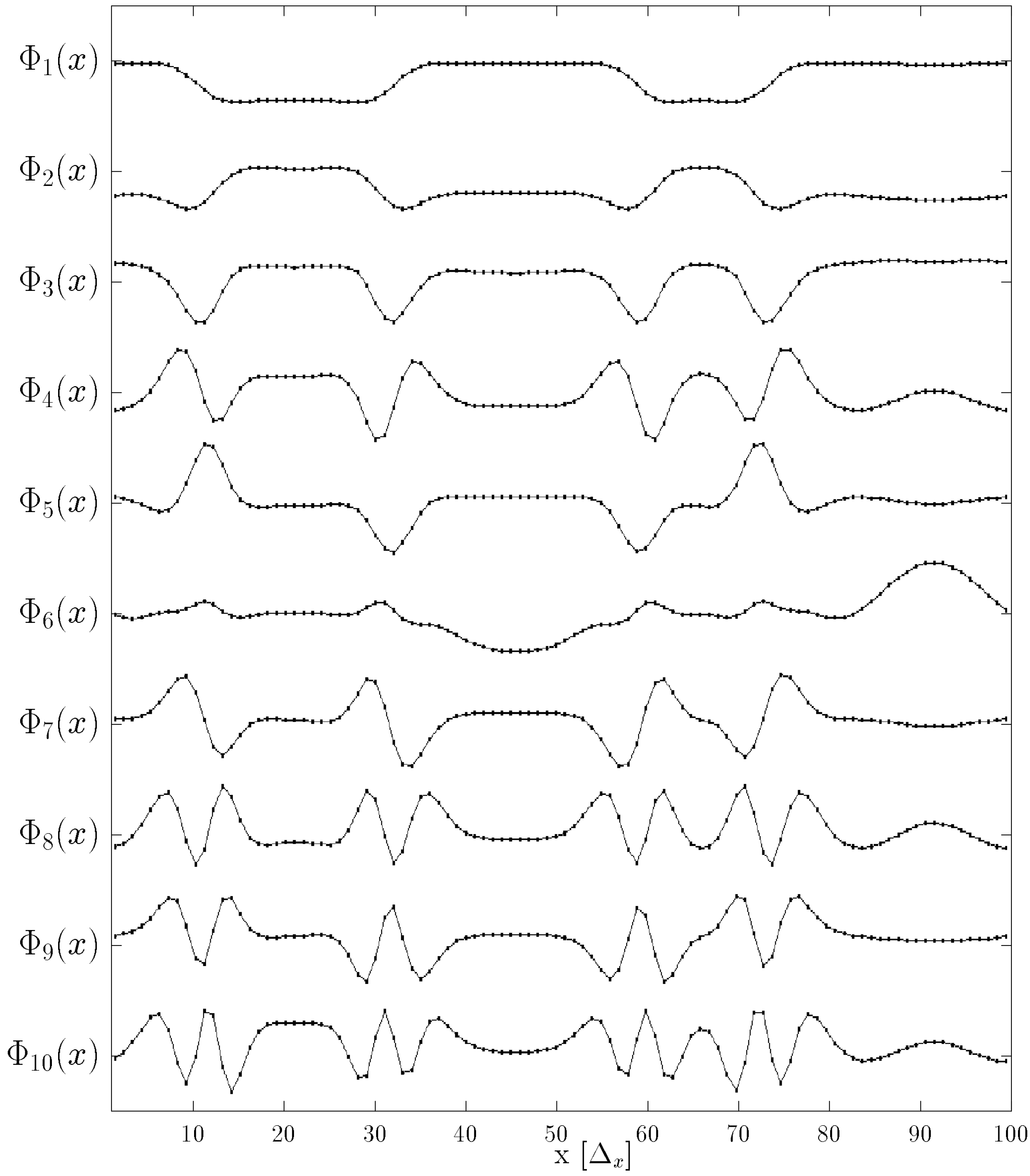

Figure 4.52: **The first ten empirical modes $\Phi_k(x)$ for data set C.**
Each mode is a vector of norm one.

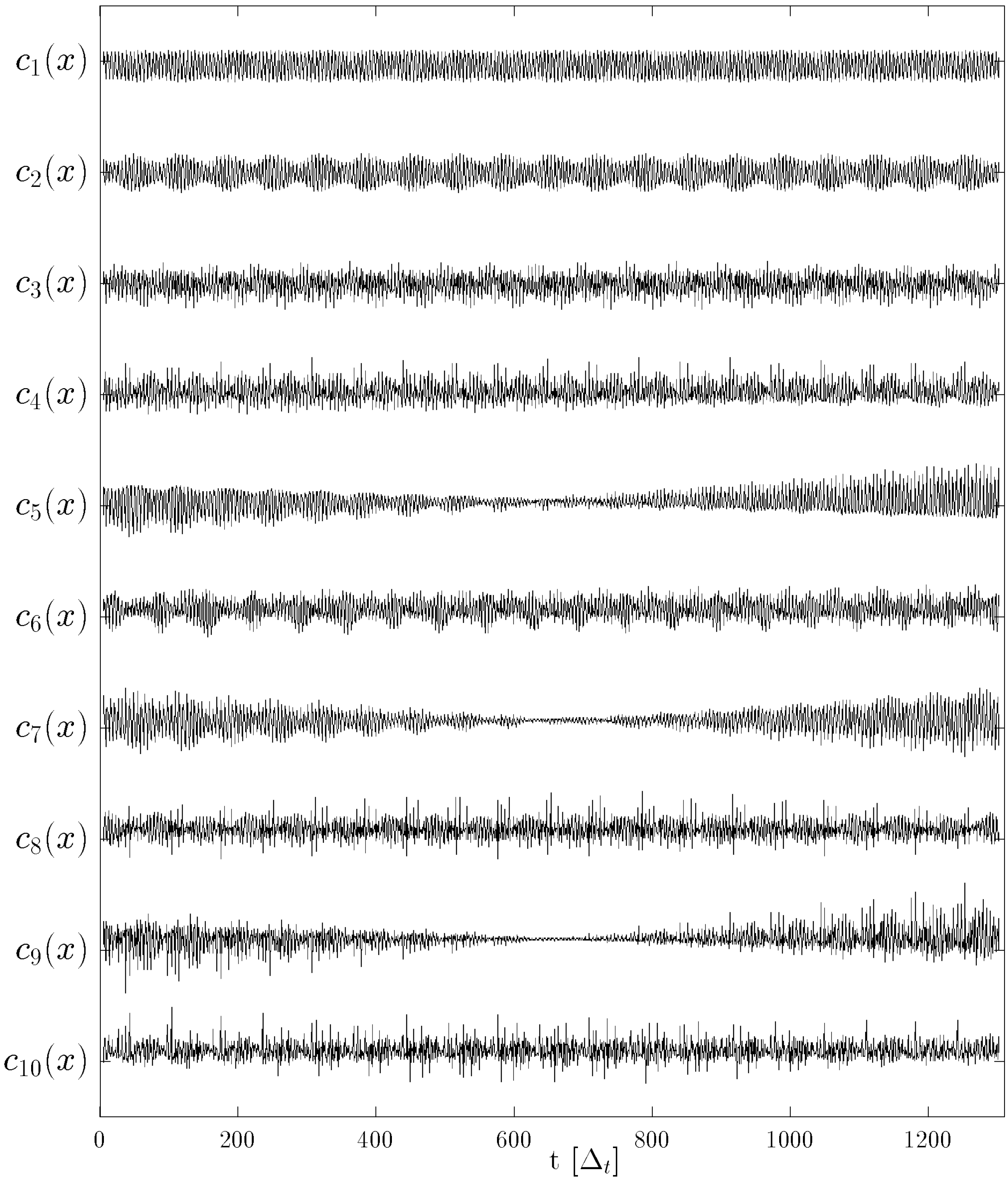

Figure 4.53: **The first ten mode amplitudes $c_k(t)$ for data set C.**
Each mode amplitude is a vector of norm one.

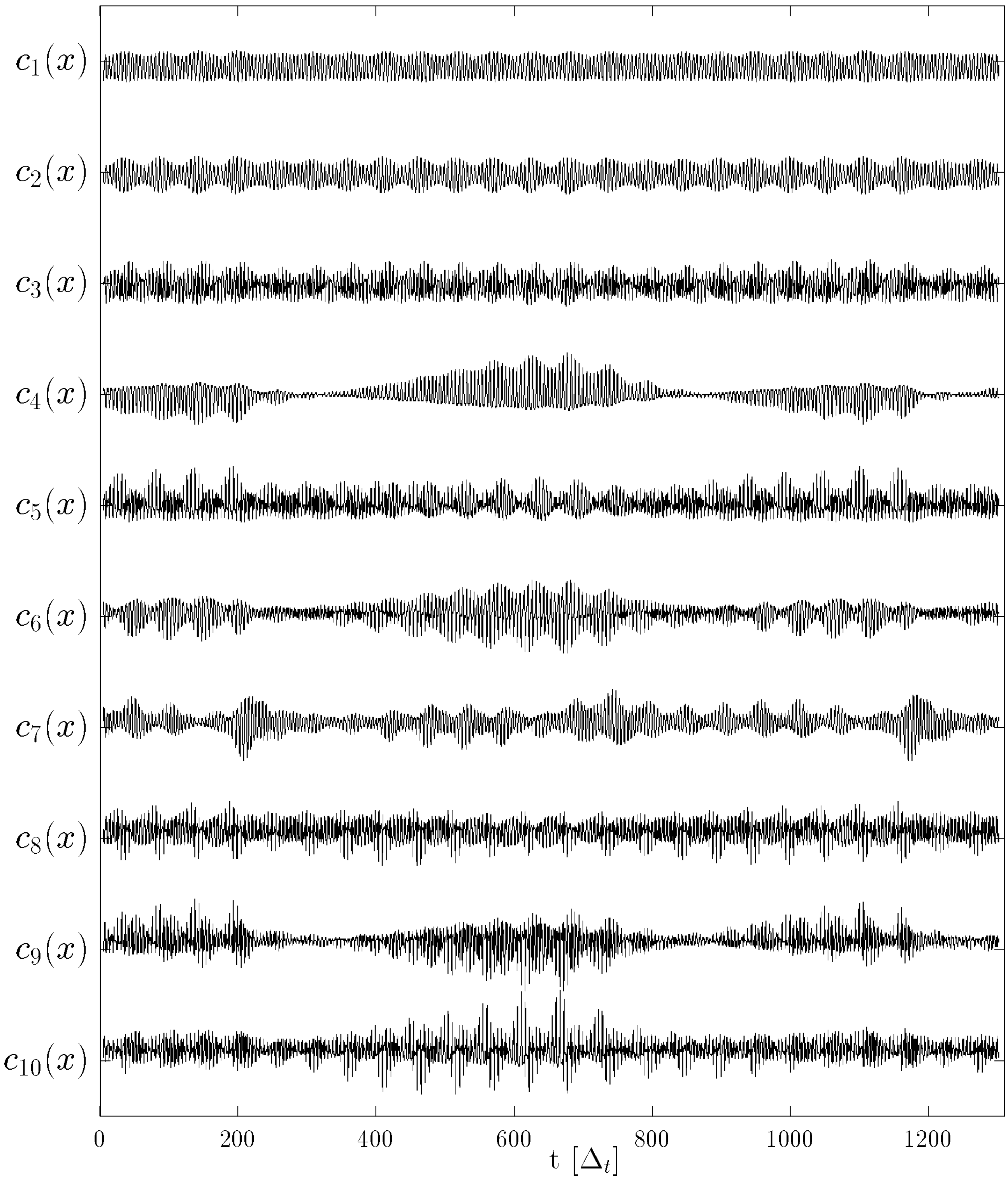

Figure 4.54: **The first ten mode amplitudes $c_k(t)$ for data set D.**
Each mode amplitude is a vector of norm one.

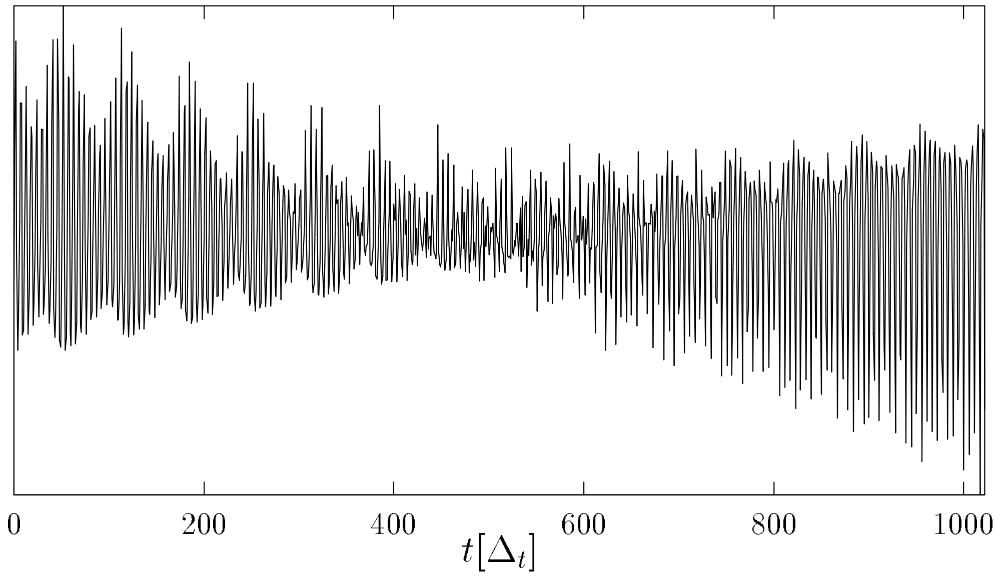

Figure 4.55: **Typical 'x-shaped' mode amplitude.**
This is the fifth mode amplitude for data set C. The corresponding singular value is 3.9 %. The mode amplitude is a vector of norm one.

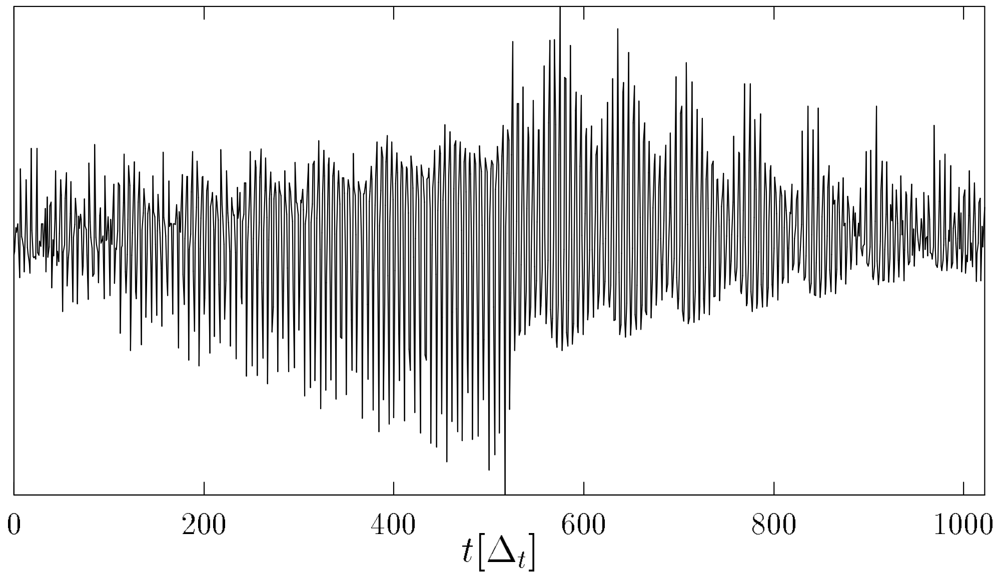

Figure 4.56: **Mode amplitude of the same data with the first and the second half of the block swapped.**
This is the result predicted by the theory.

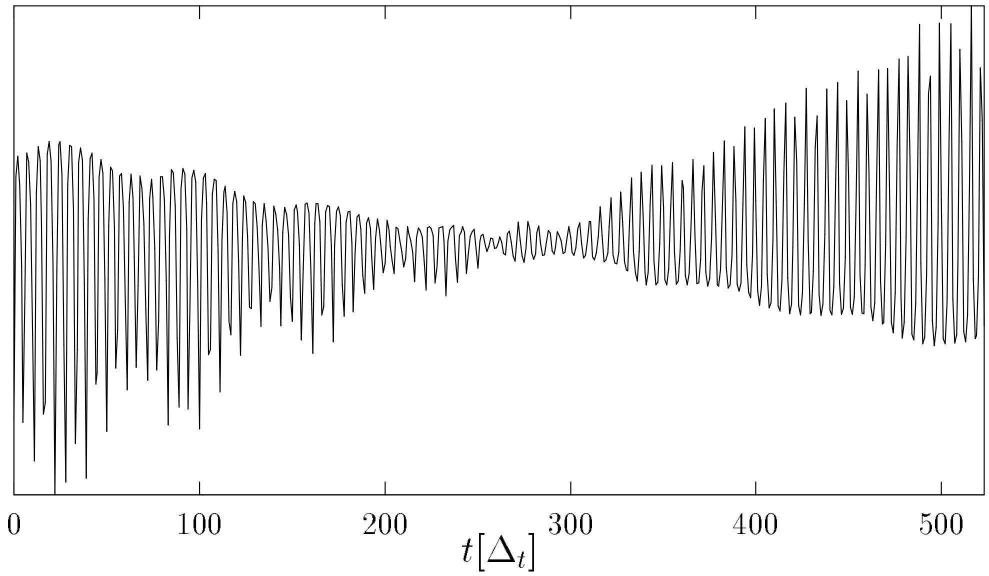

Figure 4.57: **Typical 'x-shaped' mode amplitude.**
This is the sixth mode amplitude for the second part of data set C. The corresponding singular value is 2.2 %. The mode amplitude is a vector of norm one.

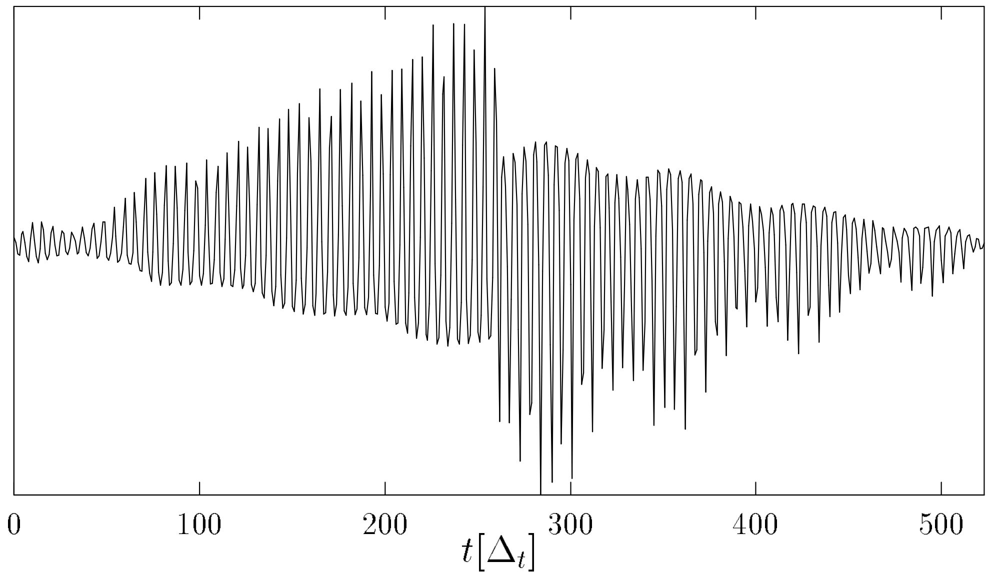

Figure 4.58: **Mode amplitude of the same data with the first and the second half of the block swapped.**
Again the result is as predicted by the theory.